

GEOSCIENCE BC PROJECT 2019-005

## **UNDERSTANDING AND MITIGATING INDUCED SEISMICITY RISK IN THE KISKATINAW AREA, BC**

**REAL-TIME MONITORING OF SEISMIC ACTIVITY IN THE KISKATINAW AREA,  
NORTHEASTERN BRITISH COLUMBIA (NTS 093P, 094A)**

---

### **GEOSCIENCE BC REPORT 2021-12**

D.W. Eaton, R.O. Salvage, K. MacDougall, T.H. Swinscoe, J. Dettmer, Z. Esmailzadeh, C. Furlong, M. Hamidbeygi, P. Igweze and P. Wozniakowska

Department of Geoscience, University of Calgary

Prepared for:

**Geoscience BC**

In original form: 2021/04/15

Revised: 2021/05/20

Revised: 2021/10/04

*The University of Calgary gratefully acknowledges the support of the following organizations:*



## Executive Summary

In certain areas, small-to-moderate (magnitudes from ~2 to 5) seismic events may be induced by hydraulic-fracturing operations. The characteristics of this seismic activity, as well as the associated ground shaking, are investigated in this project using a dense array of sensors comprised of 15 stations (13 broadband seismometers and 2 accelerometers) within the [Kiskatinaw Seismic Monitoring and Mitigation Area](#) (KSMMA). This area straddles the southern margin of the Fort St. John graben and exhibits relatively high susceptibility to induced seismicity, with abundant recorded events and numerous felt reports by local residents. The current project has involved extensive collaboration; equipment for ten of the seismograph stations was loaned to the University of Calgary by researchers based in Korea, and cooperation with oil and gas operators facilitated permitting of the stations. In addition, delivery of research results has been accelerated through collaboration with an experienced service provider (Nanometrics), who installed and operated the dense array, including troubleshooting, cloud-based data acquisition and archiving systems, 24/7 notification services and development of a comprehensive seismicity catalogue for the period 2020/01/22 to 2021/03/31 containing 9,740 events in the magnitude range  $-0.73 \leq M_L \leq 3.41$ . Data from this array improves resolution of seismic event locations, allowing detection of more numerous small events that help to characterize faults and by mapping of ground shaking in more detail than would otherwise be possible. Research results by a team of faculty members, postdoctoral researchers and graduate students at the University of Calgary encompasses the following: 1) empirical shakemaps for the ten highest-magnitude events; 2) compilation of geomechanical data aimed at understanding the role of lateral pore-pressure gradients on fault rupture; 3) preliminary probabilistic determination of source mechanism using a Bayesian approach; 4) regional geological framework; 5) analysis of temporal variations in local site response using a horizontal-to-vertical spectral ratio method; 6) detailed analysis of spatiotemporal patterns of seismicity, including an unusual period of relative quiescence from April to August, 2020 during the COVID-19 pandemic; and 7) progress in developing an updated fault database that includes KSMMA and other parts of the Western Canada Sedimentary Basin. The seismicity catalogue and peak ground acceleration (PGA) are provided with this report as supplementary data tables. It is noteworthy that ground acceleration data, calculated by differentiating ground velocity measurements from broadband seismometers, is found to be consistent with accelerations measured directly with coincident

accelerometers. In addition, raw data have been released to the public through the Incorporated Research Institutes in Seismology (IRIS) following a 91-day embargo period, thus enhancing transparency. The overall goals of this research are to inform regulatory practice and to promote safer operations by the oil and gas industry.

## Introduction

Induced seismicity that is large enough to be widely felt at the surface has occurred, albeit rarely, during or shortly after hydraulic-fracturing operations for development of unconventional hydrocarbon resources. In response to increased recognition of the potential risks of injection-induced seismicity from hydraulic fracturing, regulators in BC and Alberta have introduced so-called “traffic-light protocols” (TLPs) in certain areas (e.g., Bustin and Bustin, 2017). Within these areas, suspension of hydraulic-fracturing operations may be required in the event of an induced earthquake above a predefined red-light magnitude threshold (typically local magnitude 4.0). In 2016, the British Columbia Oil and Gas Commission (BCOGC) implemented additional requirements for ground-motion monitoring (BCOGC, 2016) in several areas, based on peak ground acceleration (PGA). One such area is the Kiskatinaw Seismic Monitoring and Mitigation Area (KSMMA) near Fort St. John (Figure 1). The initial PGA reporting threshold of 2%g ( $1g = 9.8 \text{ m/s}^2$ ) was reduced to 0.8%g in 2018 (BCOGC, 2018).

The degree of ground shaking experienced at a given location depends on various factors, including event magnitude, distance from the earthquake focus, azimuthal variations in the radiation of seismic wave energy and, in particular, amplification of ground motions due to near-surface conditions. An extensive set of direct measurements of the physical properties of the soil column has been acquired (Monahan et al., 2018) to characterize ground-motion amplification. Although this approach is the preferred method for site classification, considering the significant measured variability in the amplification of seismic ground motions in the Montney play one of the shortcomings is sparseness of data, which can be mitigated through additional monitoring instrumentation. The use of a more closely spaced monitoring array also enables the application of “shakemap” technology, a well-established method in earthquake seismology that enables rapid mapping and presentation of PGA and ground-shaking intensity (Wald et al., 1999). The deployment of empirical shakemap

technology can facilitate characterization of reasonable variability in ground shaking that has not previously been considered and capture the spatial variability of ground shaking due to all factors - not just site amplification. By providing an abundance of critical observations at close epicentral distance ranges, it can also be used to test recent models for fault activation based on precursory slow slip on faults (Eyre et al., 2019b).

In general, significant knowledge gaps remain concerning the basic physical processes of fault activation by hydraulic fracturing; filling in these knowledge gaps is essential for improved hazard assessment and risk mitigation. The occurrence of felt events due to fluid injection is thought to require the existence of an injection source, a pathway that connects fluid pressure or stress perturbation from the source to the seismogenic region, and a pre-existing fault that is capable of hosting a sufficiently large earthquake (Eaton, 2018). Fault re-activation by hydraulic fracturing is commonly attributed to an increase in pore pressure, but it may also be triggered by poroelastic stress transfer or fault loading due to aseismic creep (Bao and Eaton, 2016; De Barros et al., 2019). However, the physical process of fault activation may not be as straightforward as previously thought based on models that invoke only an increase in pore-pressure along the fault. As part of ongoing collaborative research (Eaton et al., 2019), new models are being developed, which suggest that: 1) aseismic processes (slow slip on fault systems) may play a much more significant role than previously thought (Eyre et al., 2019b), and 2) fault systems within the Fort St. John graben are segmented in such a way that rupture size is strongly influenced by the geometry of fault segments.

This project has two main components. The first involves deploying and operating a strategically located dense seismograph array consisting of 15 stations, equipped with 13 broadband seismometers and 2 accelerometers. The second component involves research, academic training and advanced analysis of the seismicity data and real-time data streams. The continuous data and derived seismicity catalogue have been made available to all researchers and participating industry sponsors during the timeframe of this project (January 22, 2020 – March 31, 2021). Following a holdback (embargo) period of 91 days, all data have been released through the Incorporated Research Institutions for Seismology (IRIS), a widely used international archival resource for seismological data. A complementary research program funded by NSERC-Alliance is underway to support expanded avenues of research that address Geoscience BC strategic priorities as well as continuation of data acquisition beyond the end of this program until December 31, 2021.

Under an agreement with the University of Calgary, instrumentation for 10 broadband seismograph stations (Trillium T120 seismometers and Taurus digitizers) was loaned to this project by a geothermal research group based in Korea. The geothermal research is led by Professors Tae-Seob Kang at Pukyong National University, Dr. Junkee Rhie at Seoul National University, and Dr. Seongryong Kim at Chungnam National University. Under a contract with the University of Calgary, a qualified service provider (Nanometrics) has augmented the Korean systems by upgrading the Taurus digitizers to the latest firmware and providing solar power, communications systems and all necessary interconnect cables. In addition to refurbishing and completing the loaned equipment kits, Nanometrics has provided from its own equipment inventory an additional 5 complete stations with either Trillium Compact posthole 20-s seismometers or Titan accelerometers, as well as turnkey installation services for all 15 stations. Through in-kind support to this project, Nanometrics has provided continuous real-time data-acquisition services including basic processing to build a seismicity catalogue. In cooperation with local oil and gas operators, locations for dense-array stations were selected by the University of Calgary within a study area measuring  $\sim 450 \text{ km}^2$  (Figure 1). The objective is to ensure that the new dense array is complementary to existing public and private arrays and will therefore provide maximum benefit in terms of geographical coverage. Nanometrics utilized the expertise of its network of contractors in BC to provide field services required to deploy and maintain all 15 stations. Nanometrics' services included:

- site surveys to confirm that selected sites meet required criteria in terms of access, solar exposure, cellular coverage, and seismic noise
- construction and installation of seismic stations using a direct-bury method, similar to the setup for long-term stations deployed by Bustin and Longobardi (2018)
- site visits as needed to restore any problematic stations to full operation
- one-time setup of the cloud-based data acquisition and archiving systems
- continuous 24/7 acquisition of all seismic waveform and state-of-health (SOH) data from all project-specific stations and all other nearby publicly available stations in NE BC
- provision of waveform data in standard miniSeed format for download at any time and kept for a period of 3 months
- processing waveforms to detect events using STA/LTA triggering and trigger association algorithms enhanced with machine learning

- separate template-matching event detection stream
- next-day review of all detected events by trained analyst on a batch-basis.
- near real-time computation and posting to the online portal of ground-motion parameters based on the signal-to-noise ratio (SNR) for each recorded event
- event notifications by email
- dedicated web portal with event download and manipulation capability
- automated extraction of event-based data for external processing
- relative relocation of the entire catalogue using high-precision processing techniques (double differencing, cross-correlation-based pick adjustment and clustering)

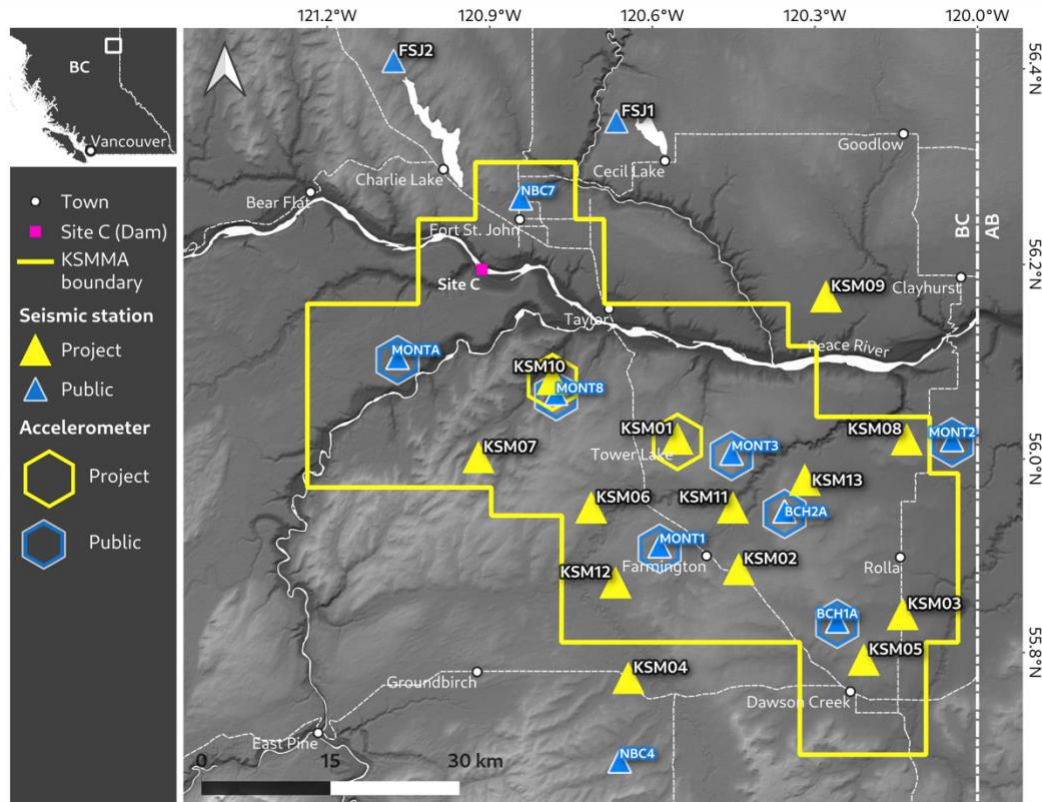


**Figure 1.** Installed seismic monitoring stations within the Kiskatinaw Seismic Monitoring and Mitigation Area (KSMMA; yellow border), northeastern British Columbia. Yellow symbols show stations installed for this project (triangles denote broadband seismometers, hexagons denote accelerometers), forming the Earth-System Observing Network–Réseau d’Observation du Système Terrestre (EO) dense array network; blue stations are previously installed public stations, managed by Natural Resources Canada (Geological Survey of Canada) or the University of Calgary. Co-located symbols (hexagon, triangle) indicate co-located sensors. Stations FSJ1 and FSJ2 are also part of the EO network but were installed in 2018. Station FSJ1 was decommissioned on August 26, 2020, but is shown for completeness as its data has been used in seismic analyses. Elevation data from Shuttle Radar Topography Mission (United States Geological Survey, 2014). WGS 84/ Pseudo-Mercator, World Geodetic System 1984 datum.

The installation and operation of the dense monitoring network in the KSMMA for this project aims to enhance the understanding of the generation of felt seismicity due to fluid injection, in particular the physical processes governing fault re-activation and the management of risk and mitigation strategies related to such events. The dense monitoring array is also useful as a tool for hazard identification, as it enables further mapping and identification of certain faults or hazards during operations that might otherwise not be identified in pre-operational planning. This is important not only for operators undertaking hydraulic fracturing completions in this area, but also for regulators and the general public so that they can improve best practices for safer operations. Accordingly, the primary research objectives of this project were to address the following questions:

- Can real-time shakemaps be used to better understand and respond to spatially variable ground shaking due to induced events?
- How can potential seismogenic structures (i.e., some, but not all, inactive geological faults) be reliably identified and mapped? How can this information be used to improve maps of geological susceptibility to induced seismicity?
- How do cohesion and frictional characteristics of active/inactive/aseismic faults compare? How is this expressed by earthquake source mechanisms?
- How can the slip-potential of individual fault segments be mapped and applied to risk assessment? For example, what is the role and significance of lateral gradients in pore pressure?
- Does local site response – amplification of ground motion due to near-surface velocity structure – vary seasonally?
- How do cumulative effects of nearby operations influence time-dependent seismic hazard? How is this expressed during a period of inactivity, during the COVID-19 lockdown in 2020?
- How can key scientific information be communicated most effectively to all stakeholders?

The ongoing focus of the research program, summarized in this report, has been to elucidate the underlying structural architecture of the fault systems and to investigate the dynamics of fault activation. This has been achieved through analysis of the raw seismograph observations and use of derived products from the dense array. Depths, focal mechanisms and types of fault movements at varying depth are valuable for interpretation and have been incorporated into research workflows. Highly qualified personnel (HQP) have been active in dissemination of research results through reports, conferences, and peer-reviewed contributions.

## Deployment Summary

For this project, 15 new seismograph stations were installed and operated, of which two were accelerometers (Figure 1). Station locations and dates of installation maintenance are summarized in Table 1, below. Some of the stations experienced minor damage due to high winds during a storm event, such as toppling of solar panels. As shown in the table, the mounting infrastructure was reinforced to mitigate this issue. All stations are actively streaming real-time data to the Nanometrics Athena portal, available for all researchers and partners of the project.

EO KSMMA Stations						
Latitude	Longitude	Station	Equipment	Date Installed	Reinforced	Reinforced
56.0209	-120.5537	<b>KSM1</b>	<b>Seismometer</b>	06-Mar-20		5-Oct-20
56.0209	-120.5537	<b>KSMA1A</b>	<b>Accelerometer</b>	06-Mar-20		5-Oct-20
55.8866	-120.4406	<b>KSM2</b>	<b>Seismometer</b>	06-May-20		8-Oct-20
55.8397	-120.1378	<b>KSM3</b>	<b>Seismometer</b>	11-Mar-20	29-Apr-20	4-Oct-20
55.9502	-120.4512	<b>KSM4</b>	<b>Seismometer</b>	10-Mar-20	28-Apr-20	5-Oct-20
55.7927	-120.21	<b>KSM5</b>	<b>Seismometer</b>	12-Mar-20		5-Oct-20
55.95	-120.7128	<b>KSM6</b>	<b>Seismometer</b>	14-Mar-20	20-Apr-20	3-Oct-20
56.002	-120.9209	<b>KSM7</b>	<b>Seismometer</b>	19-Jan-20	20-Apr-20	3-Oct-20
56.0204	-120.1305	<b>KSM8</b>	<b>Seismometer</b>	16-Jan-20	29-Apr-20	4-Oct-20
56.1673	-120.2797	<b>KSM9</b>	<b>Seismometer</b>	20-Jan-20	27-Apr-20	2-Oct-20
56.0826	-120.7844	<b>KSM10</b>	<b>Seismometer</b>	18-Jan-20	28-Apr-20	2-Oct-20
56.0826	-120.7844	<b>KSM10A</b>	<b>Accelerometer</b>	18-Jan-20	19-Sep-20	2-Oct-20
55.9502	-120.4512	<b>KSM11</b>	<b>Seismometer</b>	08-Mar-20	25-Apr-20	8-Oct-20
55.8726	-120.6678	<b>KSM12</b>	<b>Seismometer</b>	05-May-20		8-Oct-20
55.9792	-120.3173	<b>KSM13</b>	<b>Seismometer</b>	15-Mar-20	14-Apr-20	3-Oct-20

**Table 1.** Station Installation/Maintenance Record. Deployment and maintenance of the seismic array was performed for the University of Calgary under contract by Nanometrics.

With increasing operations within the KSMMA over the past decade, the number of public monitoring stations has also increased. Prior to the installation of this new dense array, nine public sensors maintained by Natural Resources Canada (NRCan; Geological Survey of Canada) existed within the KSMMA (Figure 1), along with 7 co-located accelerometers poised to better capture higher levels of ground motion from larger seismic events. Therefore, it was important that the installation of the new dense array complemented the locations of the existing stations. In particular, it was noted

that most of the public stations were positioned within a corridor orientated to the northwest, with large gaps in spatial coverage in the northern KSMMA (close to the Site C dam), and in the central area near Tower Lake and in the southwest near Farmington.

As noted previously, ten broadband seismic stations (Nanometrics Trillium T120 seismometers with Taurus digitizers) were loaned to the University of Calgary for this project by a geothermal research group in South Korea led by T.S. Kang, S. Kim and J. Rhie. Nanometrics upgraded the existing firmware on these systems and provided solar power, communication systems and interconnect cables to ensure all systems were fully operational. Installation began in January 2020, with four broadband stations and an accelerometer being successfully installed. The remaining stations were installed in March and May 2020. This dense array network supplemented two previously installed stations by the University of Calgary in 2018 in the EON-ROSE (Earth-System Observing Network–Réseau d’Observation du Système Terrestre [EO]) seismic network in this area.

Sensors were installed at existing well sites (Figure 2) with the co-operation of four oil and gas companies. The primary aim of the network was to expand monitoring capabilities in the KSMMA, in particular in the northeastern and southwestern parts of the area where prior public monitoring was sparse. However, difficulties relating to the availability of suitable sites (i.e., sites not associated with active well pads and/or having good telecommunication strength) and actual accessibility to sites meant that it was not possible to place sensors in a truly optimum spatial array. In particular, it was not possible to place sensors close to the Site C dam, an area of sparse coverage. For this reason, a decision was made to place two sensors outside of the KSMMA (KSM04 and KSM09, Figure 1) to optimize the aperture of the array, even though these sensors are at a greater distance from ongoing operations than is ideal. Stations KSM01 and KSM10 are centrally located, and both have a co-located accelerometer alongside the seismometer. The sites of the accelerometers were chosen due to their proximity to the most recent seismicity in the area, in particular a number of felt events that have occurred close to Tower Lake and Farmington (Figure 3).

Continuous seismic data from the EO network can be downloaded directly from the Incorporated Research Institutions for Seismology (IRIS) website (<https://ds.iris.edu/ds/nodes/dmc/>) following a 91-day embargo period. All station metadata are also available through IRIS. Data are released on a 24-hour basis for all stations within the network



**Figure 2.** a) Example of the footprint of a single seismic monitoring station, showing solar power panels and the top of the short borehole containing the seismometer (Nanometrics Trilium T120). The digitizer (Nanometrics Taurus) and other electronics (e.g., cables, modem, etc.) are housed within the light grey box halfway up the solar panel pole. b) Example of the depth of borehole (~30 cm) containing the buried seismometer. Sensors were buried just below the surface to reduce surface noise (e.g., meteorological, traffic, etc.).

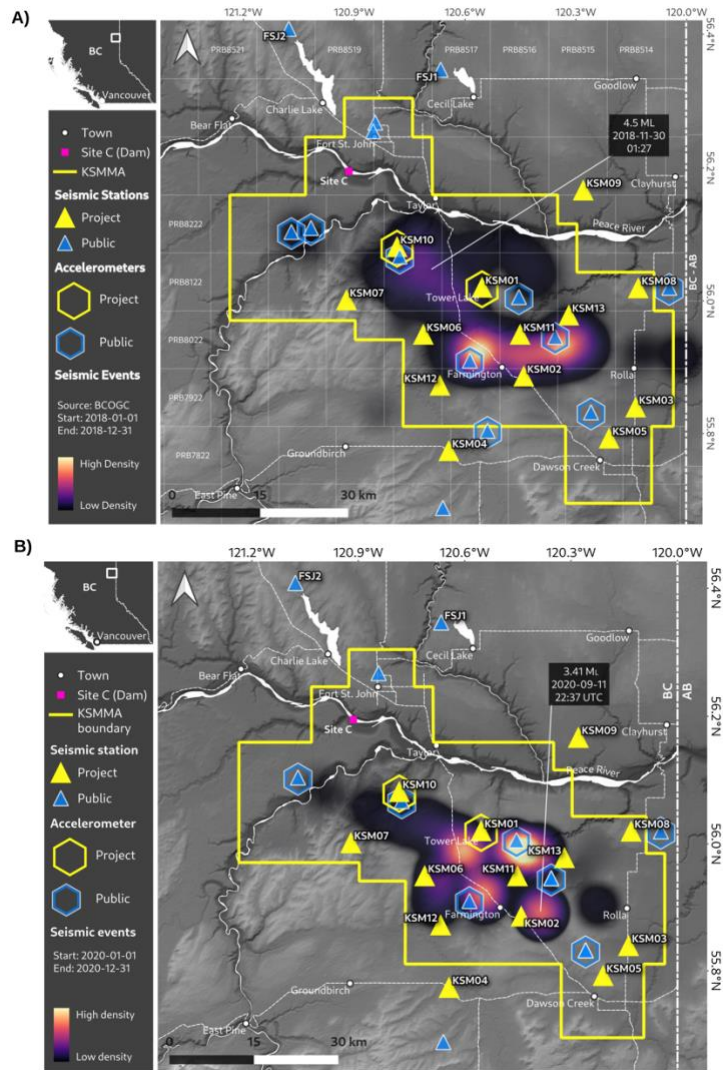


**Figure 3.** Spatial locations of seismicity concentrations within the Kiskatinaw Seismic Monitoring and Mitigation Area (KSMMA). Higher density of seismic events is indicated by brighter colours; lower density by darker colours; and no seismicity by grey. a) Seismic events recorded by Natural Resources Canada between January 1 and December 31, 2018 (data from Visser et al., 2020). Note: although the new dense array was not installed at this time, it is shown on the map for reference. The largest event in 2018, occurring on November 30 north of Tower Lake, is shown (ML 4.50). b) Seismic events recorded on the newly installed Earth-System Observing Network–Réseau d’Observation du Système Terrestre (EO) network (and incorporating data from public stations) from January 22 to December 31, 2020 (data from Nanometrics Seismic Monitoring Services, 2020). The largest magnitude event in 2020, occurring on September 11 east of Farmington, is indicated (ML 3.41). Stations FSJ1 and FSJ2 are also part of the EO network but were installed in 2018. Station FSJ1 was decommissioned on August 26, 2020, but is shown for completeness as it was used in seismic analysis prior to this. Elevation data from Shuttle Radar Topography Mission (U.S. Geological Survey, 2014). WGS 84/ Pseudo-Mercator, World Geodetic System 1984.

## Data Processing

For this project, Nanometrics provided continuous data acquisition, archiving and standard data processing of data from the EO network, incorporating data from the existing public stations in the area. This represents a significant in-kind contribution to this project to produce an accurate and well-maintained catalogue of seismic events during the recording period. The Nanometrics workflow includes event detection, event location analysis and determination of magnitudes, both automatic and through manual inspection by a trained analyst. In March 2020, Nanometrics further supplemented this workflow by deploying AI Analyst advanced processing techniques to augment the automatic processing of data. The full catalogue, including phase pick information and waveform data, as well as the continuous seismic data, is available to researchers so that they can undertake their own analysis of the seismicity.

Seismic events are initially detected from the incoming continuous seismic data using a simple short-term average over long-term average (STA/LTA) triggering algorithm, followed by a template-matching algorithm using continuously retrained modules that classify noise from events and remove unwanted signals. Then, the AI Analyst uses the support vector machine (SVM)-learning technique (e.g., Noble, 2006) to identify phase arrivals in continuous real-time waveform streams. These phase arrivals are identified by training an SVM model on historical data, as it is a supervised machine-learning approach. By converting the waveforms into over 250 features using quantities such as time and band-normalized spectrograms, a model is generated that can associate the features with P and S phases (or conversely, with noise). These can then be extracted from real-time waveforms, provided the model is applied to a network of very similar topology and geographic area for which it was trained. Additionally, the phase extraction from real-time data can be used to derive confidence measures in the phases/events detected, as well as to identify and exclude regional events. Once phases have been identified, a beamforming grid-search approach is used to identify event locations and times based on the highest likelihood P-S separation times observed at all contributing stations. Like all methods that use phase arrival times and rely on a velocity model, focal depth is the least well constrained hypocentral parameter and has the largest uncertainty (Eaton, 2018). Absolute depth uncertainties for the preliminary hypocentres in our catalogue depend on the signal-to-noise ratio and the number of stations at which detections were observed. For a given event, depth uncertainty of the preliminary hypocentre is generally on the order of ~500m (or more). As is typical for published cross sections of

induced seismicity, positional error bars are not plotted in this report, for visual clarity. We therefore caution against over-interpretation of the preliminary focal depths.

Event locations are further refined using a double-differencing algorithm to produce high-precision locations (Figure 4). This algorithm uses a one-dimensional (1-D) velocity model and parameters such as cross-correlation specific thresholds, and some parameters relating to event pairing. This approach reduces errors associated with the velocity model and pick placement by relocating events to minimize a) the travel time differences between co-located event pairs and b) the pick time differences between cross-correlated waveforms from co-located event pairs. A precision estimate is then derived by bootstrapping the input catalogue and quantifying the resultant hypocentre distribution. The 1-D velocity model used has been specially derived for the KSMMA (provided by the BCOGC) based on sonic logs (compressional and shear) and formation tops and calibrated using events detected on local networks from a number of operators within the KSMMA. The velocity model is presented in the Supplementary Materials that accompany this report. As seen in Figure 4b, high-precision hypocentres locate this set of events approximately at the level of the Montney Formation (~ 2 km).

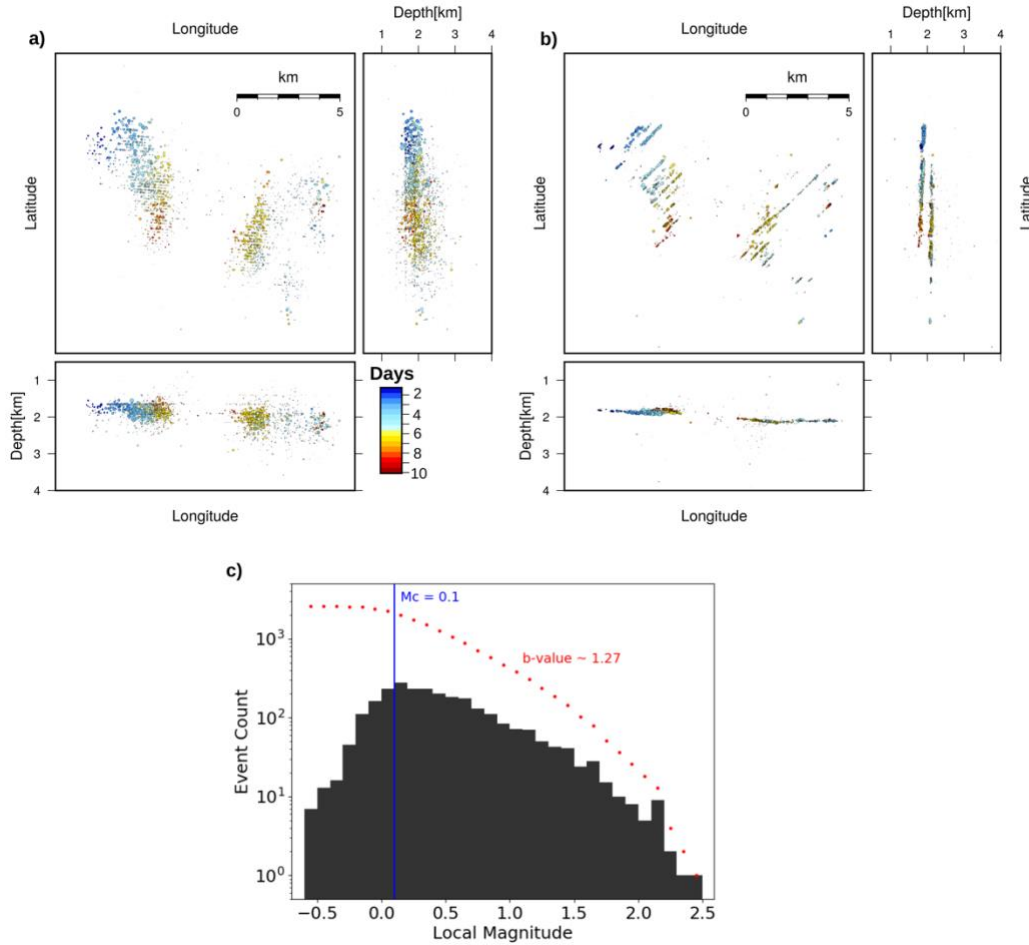
Local magnitudes ( $M_L$ ) were originally calculated using a form of the Hutton and Boore (1987) magnitude formula, which was developed for events in southern California that are detected on stations with up to 100 km epicentral distance. This scale is based upon the Wood-Anderson conversion of seismic sensors using the peak S-wave amplitude measurement. We also calculated the local magnitude using the Babaie-Mahani and Kao (2020) formula, which is also based upon the Wood-Anderson conversion of seismic sensors, but has been specifically calibrated for the KSMMA. This calculation uses the maximum peak amplitude on the vertical component of the seismometer.

## **Recorded Seismicity**

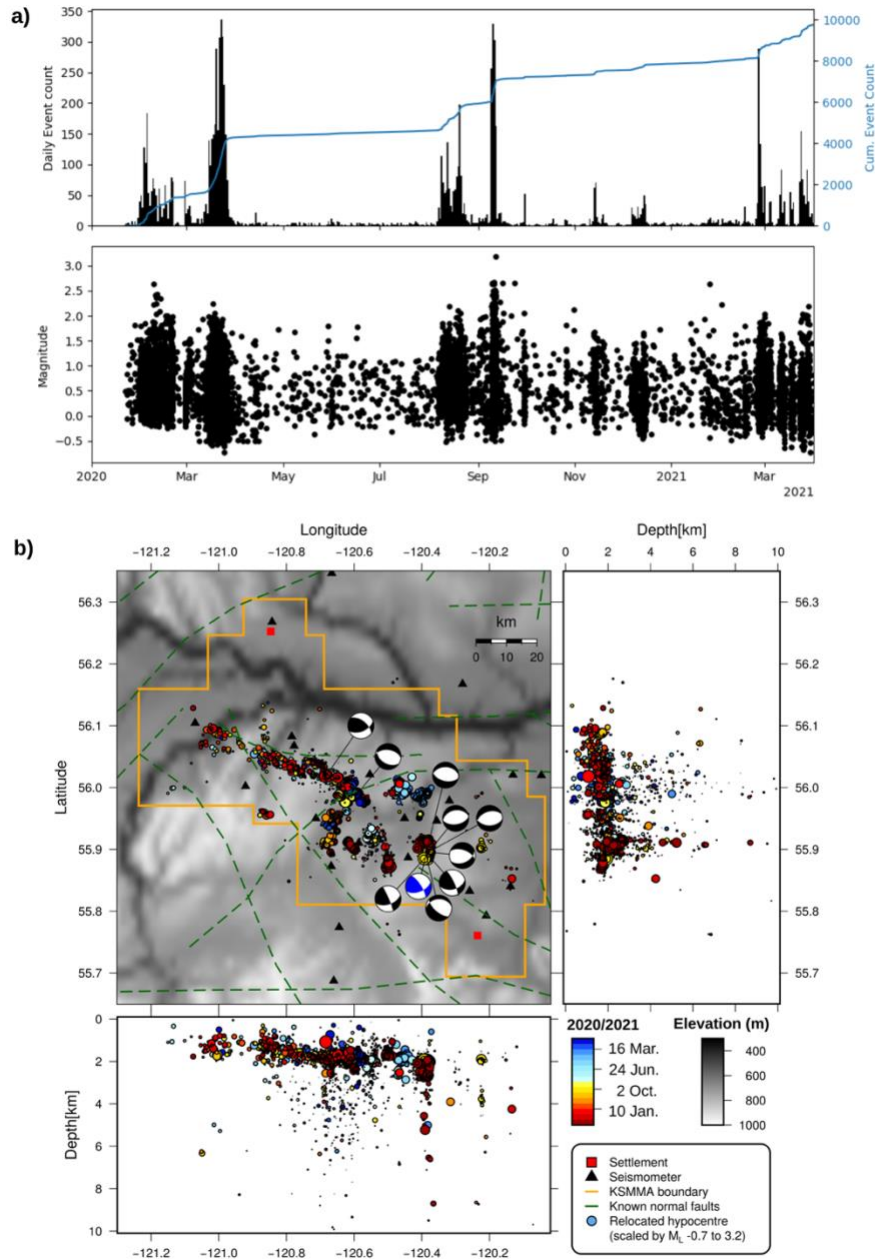
The first data from the EO network were received on January 22, 2020. At that time four stations had been installed; the remaining stations were installed in the spring (March and May 2020). From 22 January 2020 to 31 March 2021 (inclusive), 9,740 events were detected in the KSMMA using the EO network and available public stations, with 9,484 events reporting high-precision relocations. All events were automatically detected and have been manually verified by an expert at Nanometrics.

Figure 5a (upper) shows the temporal evolution of detected seismicity from 22 January 2020 to 31 March 2021, both daily and cumulative. Distinct heightened periods of seismicity can be observed, particularly in February, March, August and September of 2020, and again in February and March of 2021. This reflects ongoing operations in the area during these times. A clear period of quiescence is observed from April until August, representing the unprecedented situation that occurred in 2020 with the lockdown of people, businesses and cities due to the COVID-19 pandemic.

Spatially, seismicity in the KSMMA appears to occur within a band orientated to the northwest (Figures 3, 5b). Seismicity in 2020 appears to occur within a region that is spatially distinct from seismicity in 2018 (Figure 3b versus 3a), but this may be due to the fact that there have been significantly fewer operations in 2020 due to the COVID-19 pandemic. Interestingly, the largest event in 2018 ( $M_L$  4.5, November 30) occurred to the north of Tower Lake, away from the densest cluster of seismic events (Figure 3a). During the period of investigation (22 January 2020 to 31 March 2021), the largest event occurred on September 11 ( $M_L$  3.41, Hutton and Boore, 1987;  $M_L$  3.2 Babaie-Mahani and Kao, 2020) in the southern area of the KSMMA (Figure 3b), but again away from the densest cluster of events. Assuming this seismicity is associated with ongoing hydraulic fracturing operations, this suggests that the largest magnitude events do not necessarily occur near the densest activity. Moreover, given that the largest event in 2020 did not occur in the same cluster as the largest event of 2018, it appears that the occurrence of  $M_L$  3–4+ events is not confined to a single region.



**Figure 4.** Spatial cluster of 2,098 seismic events that occurred over ~10 days at the end of March 2020 in part of the Kiskatinaw Seismic Monitoring and Mitigation Area. This example of preprocessing conducted by Nanometrics shows the difference between **a)** their calculated standard locations of seismic events and **b)** their calculated high-precision locations of seismic events using a double-differencing algorithm. Latitude and longitude values are not shown in order to maintain confidentiality of this specific well. High-precision locations clearly denote linear features, which appear to correlate temporally with ongoing hydraulic fracturing operations in the area. High-precision event depths place the seismicity approximately at the target reservoir (Montney) level (~ 2 km). **c)** Semilogarithmic plots of non-cumulative (histogram) and cumulative (red dotted line) magnitude-frequency distribution for this cluster. The catalogue magnitude of completeness ( $M_c$ ) was calculated using the method of Wiemer and Wyss (2000), and the  $b$ -value (negative slope of the cumulative distribution) was calculated using the maximum-likelihood method of Aki (1965).



**Figure 5.** Evolution of seismicity detected since installation of the Earth-System Observing Network–Réseau d’Observation du Système Terrestre (EO) network within the Kiskatinaw Seismic Monitoring and Mitigation Area (KSMMA) from 22 January 2020 until 31 March 2021 ( $n=9740$ ) **a)** Time series of events detected. Upper panel denotes event count per day and the cumulative event count through time; lower panel denotes local magnitude ( $M_L$ ) of each event (Babaie-Mahani and Kao, 2020). **b)** Spatial evolution of seismicity (coloured by time), which appears in distinct spatial clusters. Red squares denote settlements: Fort St. John in the north and Dawson Creek in the south. The majority of seismic events have a preliminary focal depth of 1–2 km, but further study is required to refine these calculated depths (see Figure 4b). Known normal faults within the KSMMA are shown, taken from Furlong et al. (2020). Focal mechanisms, calculated using P-wave polarity estimates and P/S wave amplitude ratios, are shown for the ten largest events to occur during the recording period (largest event shown in blue).

Clusters of seismicity are also seen in focal depth plots (Figure 5b), with most events showing preliminary focal depths between approximately 1 and 2 km, although a number of smaller events do extend down toward the basement (which lies at an average depth of ~4.0 km across the KSMMA). Target formations for hydraulic fracturing within the KSMMA (e.g., upper and lower members of the Montney Formation) typically lie between 2.0 and 2.5 km (total vertical depth). However, due to uncertainties in absolute focal depth noted above, further study and refinement of depth estimates using other methods (e.g., Poulin et al., 2019) are needed before carrying out any detailed geological interpretation of the hypocentre distributions in depth. We remark that a recent application of the new method of Poulin et al. (2019) in the Montney play resulted in re-location of all events to the Montney level or deeper (Riazi et al., 2020).

As well as detailing the target formations at depth, the spatial evolution of seismicity allows the detailing of fault and fracture growth in near real-time (Figure 4). High-precision locations (using double-differencing techniques) reveal clear planar features associated with active hydraulic fracturing operations. The average strike orientation of the features defined by the seismicity trends is N62°E, which is oblique to the average SHmax direction in this area (N45°E; Fox and Watson, 2019). The average SHmax direction defines the expected direction of growth of hydraulic fractures. Figure 4 shows a spatial cluster of 2,098 seismic events occurring over ~10 days at the end of March 2020. In Figure 4a, events appear scattered spatially, although there is some degree of order to the events temporally, with the oldest events occurring to the northwest. Following relocation using double-differencing methods (Figure 4b), clear planar features are evident, which appear to ‘grow’ with time toward the southwest. Two distinct populations are identified, which appear to be simultaneously active. The largest planar feature in the southeast is approximately 3 km in length, allowing a better understanding of the extent of ongoing operations in the area, in lieu of having detailed injection data from individual operators.

The installation of the majority of seismic sensors in the EO network in March was generally accompanied by a reduction in the minimum detected magnitude at this time (Figure 5a, lower panel). With four stations installed in January (in addition to the public sensors in the area), the minimum detected magnitude was close to  $M_L$  0. In March 2020, this was significantly reduced, with the EO network (when combined with available public stations) now recording some events close to  $M_L$  -1. It should be noted that the minimum detected magnitude depends on a number of factors, including

noise levels and seismicity level, leading to some apparent fluctuations that are unrelated to the station density. This was partly due to the installation of stations creating a denser network, but also reflects the introduction of the AI Analyst processing tool by Nanometrics, which incorporated machine-learning techniques to further refine  $M_L$  for detected events. The estimated magnitude of completeness ( $M_c$ ) calculated using the maximum curvature method of Wiemer and Wyss (2000) is 0.17 (Figure 6), suggesting that all events larger than this are detected. This is significantly lower than the estimated  $M_c$  of 0.6 that was postulated in the funding proposal to Geoscience BC and is in part due to the optimized network design.

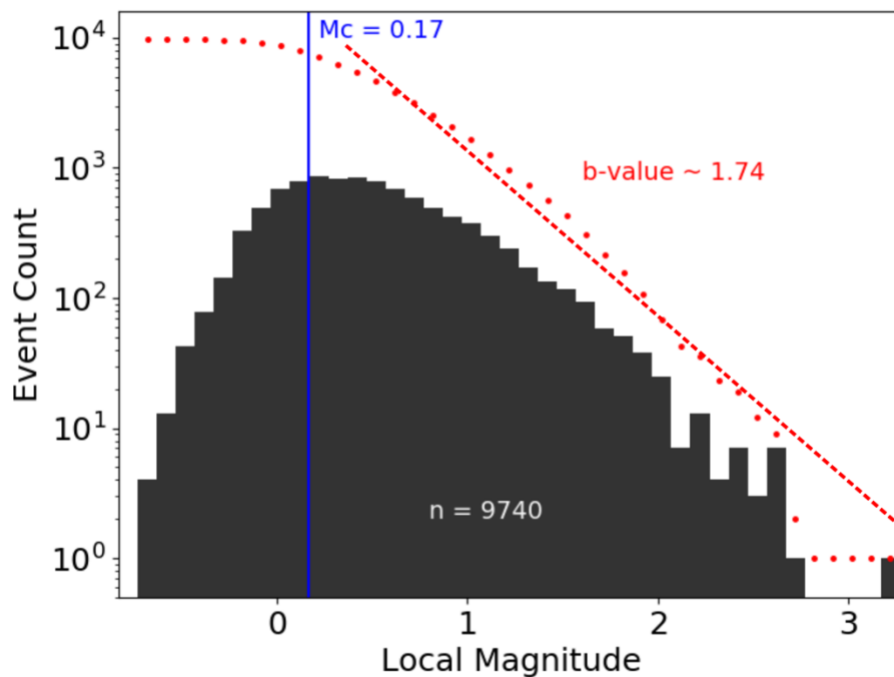


**Figure 6.** Semilogarithmic plots of non-cumulative (histogram) and cumulative (red dotted line) magnitude-frequency distribution for all events detected in the KSMMA from 22 January 2020 to 31 March 2021 ( $n=9740$ ). Red dashed line shows line of best fit. The catalogue magnitude of completeness ( $M_c$ ) was calculated using the method of Wiemer and Wyss (2000), and the  $b$ -value (negative slope of the cumulative distribution) was calculated using the maximum-likelihood method of Aki (1965). Magnitudes were estimated using the formula of Babaie-Mahani and Kao (2020). The estimated magnitude of completeness ( $M_c$ ) is 0.17, and the estimated  $b$ -value is 1.74.

Seismicity directly relating to hydraulic fracturing (operationally induced seismicity) has been shown to have a higher  $b$ -value ( $\sim 2$ ; Maxwell et al., 2009; Eaton and Maghsoudi, 2015), indicating the dominance of many small earthquakes in comparison to large events. In comparison,  $b$ -values for natural seismicity in the northern hemisphere is approximately 1.0 (El-Isa and Eaton, 2014). The estimated  $b$ -value for events detected in KSMMA, from the EO network and available public station

data, is 1.74 (Figure 6), which suggests that the seismicity has characteristics associated with anthropogenic origins. Schorlemmer et al. (2005) suggested that the  $b$ -value may be influenced by the tectonic stress regime, and that a value greater than 1.1 is indicative of normal faulting regimes. The KSMMA is strongly influenced by the Fort St. John graben complex, an asymmetrical half graben that has also undergone significant strike-slip and rotational movement upon reactivation of the basement faults in the area (Barclay et al., 1990), with a number of normal faults associated with the extension of the graben falling within the KSMMA (Furlong et al., 2020; Figure 5b). The estimated  $b$ -value for the entire sequence appears to be strongly influenced by a period of quiescence that occurred in the KSMMA in 2020 in relation to the COVID-19 pandemic and the subsequent fall in stock prices of the companies working in this region. The estimated  $b$ -value during this time (from April to August 2020) was 1.96 (Salvage and Eaton, 2021), significantly higher than the estimated  $b$ -value for the entire catalogue of detected events ( $b$ -value = 1.74).

The largest magnitude event to occur during our recording period occurred on September 11 at 22:37 UTC with an estimated  $M_L$  3.2 (Babaie-Mahani and Kao, 2020;  $M_L = 3.41$  for Hutton and Boore, 1987), following which operations in the area were suspended in accordance with the BCOGC's TLP introduced for the KSMMA in 2018 (BC Oil and Gas Commission, 2018). Due to the COVID-19 pandemic and the subsequent fall in oil and gas stock prices, operations only restarted in the KSMMA at the beginning of August 2020, following approximately four months of almost total quiescence beginning in April (Figure 5a). The event on September 11 occurred quickly following this resurgence of activity. A total of 73 precursory events occurred over approximately four hours, with events locating within a small spatial extent (~300 by 150 m). These events are probably directly related to ongoing operations in the area based on the correlation in space and time of events and injection. Events within this precursory sequence had magnitudes between  $M_L$  0.2 and 2.6, and were all located at depths of approximately 2.05 km. The mainshock was located at a similar depth of 2.01 km (Salvage and Eaton, 2021). A fully non-linear Bayesian centroid moment tensor solution suggests that this event was dominated by strike-slip movement (Salvage et al., 2020).

Focal mechanisms were estimated for the ten largest events to occur during our recording period using P-wave polarity information, as well as P/S wave amplitude ratios. A diverse range in focal mechanisms is observed, even within a small spatial extent (e.g. the cluster containing the largest event recorded in the south of KSMMA). This suggests that the slip regimes within the KSMMA are

diverse, as has been previously postulated (e.g., Salvage, Jia and Eaton, 2020) related to the geographic (and geological) location of the KSMMA.

## Ongoing Research

### *Empirical shakemaps*

Shakemaps are a well-established method in earthquake seismology that enable rapid mapping and presentation of peak ground acceleration (PGA) and shaking intensity (Wald et al., 1999). If densely spaced seismograph stations are available in the area of an induced event, a shakemap can be computed automatically by interpolating measured peak ground acceleration values at each station. Figure 7 illustrates the concept, based on waveform recordings from a  $M_L$  3.14 event on 2020-09-11 at 22:37:27. The relocated hypocentre for this event (this study) is 55.894019N 120.38304W at a focal depth of 1.057 km. The magnitude of  $M_L$  3.14 was calculated use the local magnitude method of Babaie Mahani and Kao (2020).

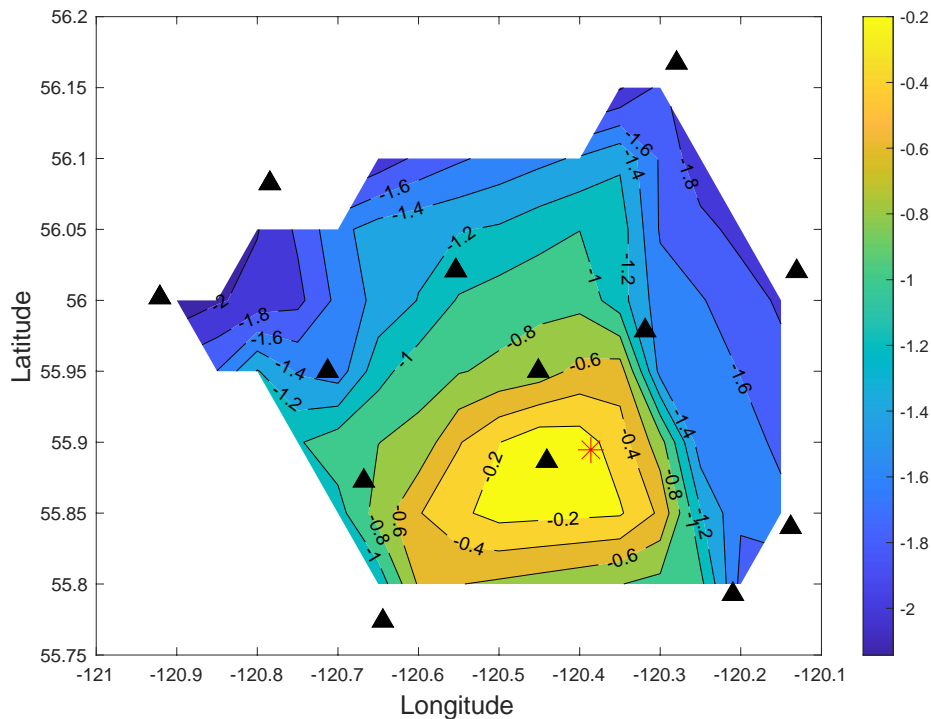


**Figure 7.** Empirical shakemap for the 2020-09-11  $M_L$  3.14 earthquake, based on peak ground acceleration (PGA) values measured at KSM stations and FSJ2. The contours show  $\log_{10}(\text{PGA})$  in units of  $\text{m/s}^2$ . Black triangles show stations, and the red symbol shows the event epicentre.

To compute an empirical shakemap, the peak ground acceleration (PGA) value for each station was calculated by applying the instrument response correction to transform the recorded ground motion data to units of acceleration ( $\text{m/s}^2$ ), and filtering between 1 Hz and either 45Hz (FSJ2) or 85 Hz (all KSM stations). Two of the KSM stations (KSM01 and KSM10) are equipped with Titan accelerometers as well as Trillium Compact 20s seismometers. The remaining stations are only seismometers, which measure velocity, but this can easily be converted to acceleration by taking the time derivative. The maximum 3-component PGA value (i.e., the maximum vector amplitude) was calculated by taking the square root of the sum of the squares of the east, north and vertical components. No site correction was applied to the computed PGA value – this will be considered for future work. The ground motion values were interpolated between stations using a linear interpolation algorithm in MATLAB. In cases where coincident seismometer and accelerometer were available, the average PGA value was used.

For comparison with previous studies, Figure 8 shows calculated PGA values versus hypocentral distance for the largest 10 events in this study (red and green symbols) and for  $M_L > 2.5$  events from the Septimus and Graham areas (black dots), based on Babaie Mahani and Kao (2018). The average magnitude for the set of events from Babaie Mahani and Kao (2018) is  $M_L$  2.81, whereas for this study the average magnitude is  $M_L$  2.94. As expected, for this study the highest ground motions are observed for the largest event ( $M_L$  3.14). However, the ground motions recorded in this study appear to be slightly, but systematically, larger than those reported by Babaie Mahani and Kao (2018). This difference may reflect different methods used for data preparation or, speculatively, they could indicate that ground motions in the south-central KSMMA area where the largest number of felt reports have been obtained (Tower Lake and Farmington; S. Venables, pers. comm. 2020), are higher than average for a given magnitude. Indeed, ground-motion amplification at particular localities is already known to be a significant factor (Monahan et al., 2018; 2019; 2020). Further research is required to evaluate these effects based on direct measurements of ground motion. Empirical shakemaps for the largest 10 events for the catalogue in 2020 are presented in Appendix 2.

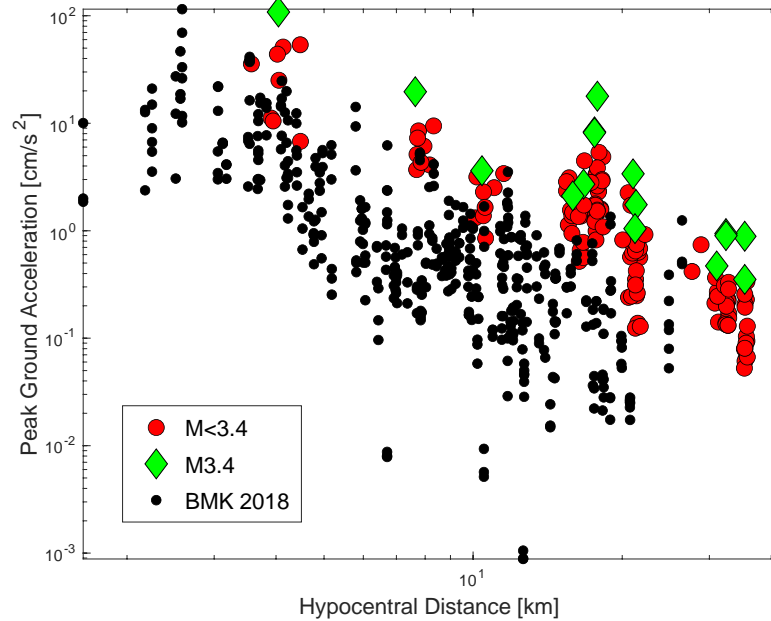


**Figure 8.** Graph of peak ground acceleration (PGA) versus hypocentral distance for the ten largest events from this study (red and green symbols), compared with  $M_L > 2.5$  events from the Septimus and Graham areas (Babaie Mahani and Kao, 2018). The green symbols are for the event shown in Figure 7. In the legend, M denotes  $M_L$  using the Hutton and Boore (1987) scale, used here for comparison with the results from Babaie Mahani and Kao (2018).

### *Effects of pore pressure*

This ongoing research component investigates the effects of pressure partitioning on induced seismicity associated with fluid injection, through integrated reservoir modeling and fault-slip-potential (FSP) analysis. A structural model of the study area has been constructed based on available data. The study area encompasses the Septimus field, including the November 2018 earthquake location, and covers a large part of the KSMMA area. Various reservoir data were analyzed to construct the reservoir model, including petrophysical, geomechanical and hydrodynamic data. Reservoir pore pressure was extracted from diagnostic fracture injection tests (DFITs) and downhole pressure measurement reports from Halfway to Belloy formations. Similarly, stress data were extracted from DFIT and hydraulic fracturing operational reports for the Montney Formation. Public data were used to construct the provisional fault model used in this study.

Using sonic and density logs, we estimated elastic rock properties. The discontinuities in the distribution of reservoir geomechanical parameters seem to follow the location of previously mapped faults (Figure 9). Figures 9c and 9d show the pore pressure distribution for the Upper and Middle Montney formations. The distribution of pressure compartments and discontinuity patterns show a

good match to that found by Fox and Watson (2019), suggesting that reservoir pressure compartments are fault-bounded.

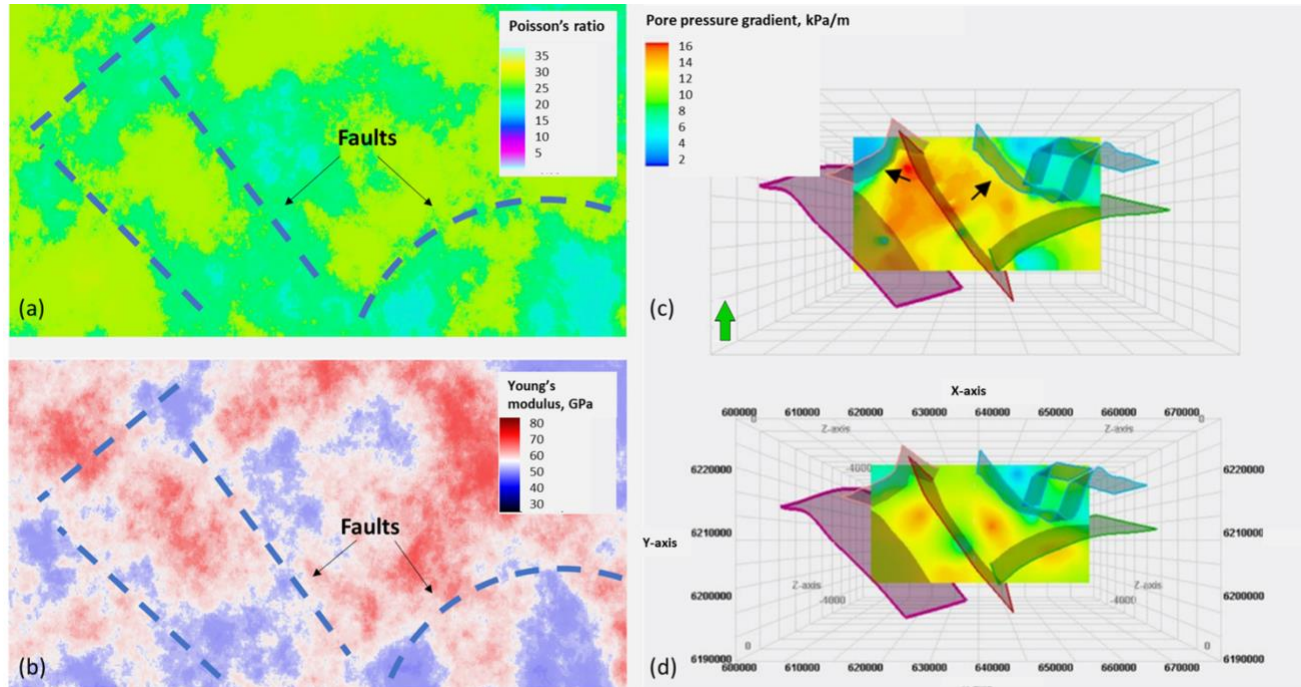


**Figure 9.** (a) Poisson's ratio at the Upper Montney level in the Septimus area (a region measuring 56 km x 30 km in the central part of the KSMMA). (b) Young's modulus at the Upper Montney level. (c) Pore-pressure gradient at Upper Montney. (d) Pore-pressure gradient at Middle Montney formation.

### *Regional geological framework*

The Lower Triassic Montney Formation is one of western Canada's most lucrative unconventional oil and gas reservoirs with an estimated marketable potential of 449 Tcf natural gas, 14.5 billion barrels of natural gas liquids (NGLs), and 1.13 billion barrels of oil (National Energy Board, 2013). The formation extends across western Alberta and Northeastern British Columbia at depths ranging from 700m in the northeast to 3500m in the southwest below the surface and can reach up to a total thickness of over 300m. Due to its vertical thickness, several layers of well can be drilled to improve the production of the well/pad, and a stacked target development strategy is commonly used.

The Montney Formation has commonly been referred to as the "Monotoney" due to its seemingly monotonous appearance, with much of the formation consisting of gray planar laminated

siltstone. However, sedimentological heterogeneities are prevalent throughout the formation as facies variability and depositional processes subtly change both spatially and temporally. In turn, these subtle heterogeneities are inherently linked to geomechanical and reservoir properties and likely play an important role in understanding the behavior of hydraulic fracturing within different zones of the formation.

To understand and describe geological heterogeneities, a multidisciplinary approach will be taken. First, constructing a stratigraphic framework is vital to understanding facies distributions, heterogeneities, stratigraphic architecture, and basin evolution. Multiple studies have been published investigating Montney stratigraphy, with many subdividing the interval into three main members: the Lower Montney, the Middle Montney, and the Upper Montney (e.g., Davies et al., 2018). Additional subdivisions have been proposed based on lithostratigraphic context (Zonneveld and Moslow, 2018) and sequence stratigraphic interpretations (e.g., Crombez et al., 2016; 2017; Davies et al., 2018). Although many of these subdivisions are comparable between studies, some discrepancies occur. Therefore, stratigraphic tops and small-scale subdivision related with flooding surfaces have been picked using petrophysical well logs from wells across the greater KSSMA region and have been compared to previous studies. Cores from Alberta and British Columbia have been and will be integrated into the stratigraphic framework to verify and modify the working stratigraphy. A facies analysis will be conducted on each core to describe grain size, sedimentary structures, trace fossils, and body fossils. An example facies photos and distribution are provided in Figure 10. Based on the core descriptions, vertical and lateral facies variability will be described, and facies will be correlated to petrophysical logs to produce facies maps. The stratigraphic correlations and maps produced will provide vital geological context and regional background to other studies funded by this grant.

Complimentary to constructing a stratigraphic framework and facies analysis, the core will be investigated for fractures and structural fabrics, which occur both naturally and as a result of cutting the core (induced). A variety of fractures and structural fabrics have been described from the Montney Formation, with microjoints along bedding planes being the most common. Studies on structural fabric of the Montney have been conducted within the Farrell Creek Field (Rogers et al., 2014; McLellan, 2014), Middle Montney of the Karr-Kakwa area (Davies et al., 2014, 2016), and other non-disclosed locations (Gillen et al., 2019). However, none of these studies have integrated detailed geological attributes in the dataset. Therefore, detailed lithological description, associated sedimentary structures,

and overall facies will be identified and described for each microjointed bedding plane. Other data collect include core depth, number of microjoints on the bedding plane, maximum and minimum distance between each microjoint, and preservation of each microjointed sample. The number of microjointed bedding plane surfaces and the number of core pieces per half-meter length are also recorded to determine mechanical facies. A simplified display of this data is shown in Figure 10, and shows that there is an increased frequency of microjoints and core pieces within the Middle Montney Formation. Currently, two cores from Alberta, located just east of KSSMA, have been investigated for microjoint distribution.

### *Bayesian source inversion*

This research component focuses on the application of Bayesian source and stress inversion to better understand rupture processes and how these relate to the regional stress field. The BEAT software (Vasyura-Bathke et al., 2020) is used to constrain centroid moment tensor (CMT) solutions of earthquakes with  $M_L \geq 3.0$ . The BEAT software is based on waveform inversion and includes the Lune parameterization of moment tensor sources, to better constrain complex source processes and avoid parameterization bias. Once a catalog of CMT solutions is generated, we consider Bayesian stress inversion. In particular, the uncertainty of moment tensor (MT) solutions is propagated through the Bayesian stress inversion by considering the Bayesian output of the MT inversion as input for the stress inversion. This approach provides a more rigorous estimate of stress than is possible with the current practice of making assumptions about MT uncertainty when creating the stress-inversion input. By applying clustering methods to the MT solutions in space, the aim is to resolve the spatial variability of stress in the region. Estimates of the spatial variability of stress will inform an interpretation of how induced events relate to the tectonic setting and will be combined with spatial rupture models for events of  $M_L \geq 4.0$ . Probabilistic CMT results for the Nov 30, 2018  $M_L 4.2$  event in the Septimus area using BEAT analysis is presented in Figure 11. Notably, waveform fits show variance reduction of up to 90%. These fits are combined with a CMT model that requires only modest isotropic and CLVD components, indicating that the complex waveforms can be explained with a simple rupture model. Therefore, this event likely activated an existing tectonic fault with thrust mechanism that is nearly planar.

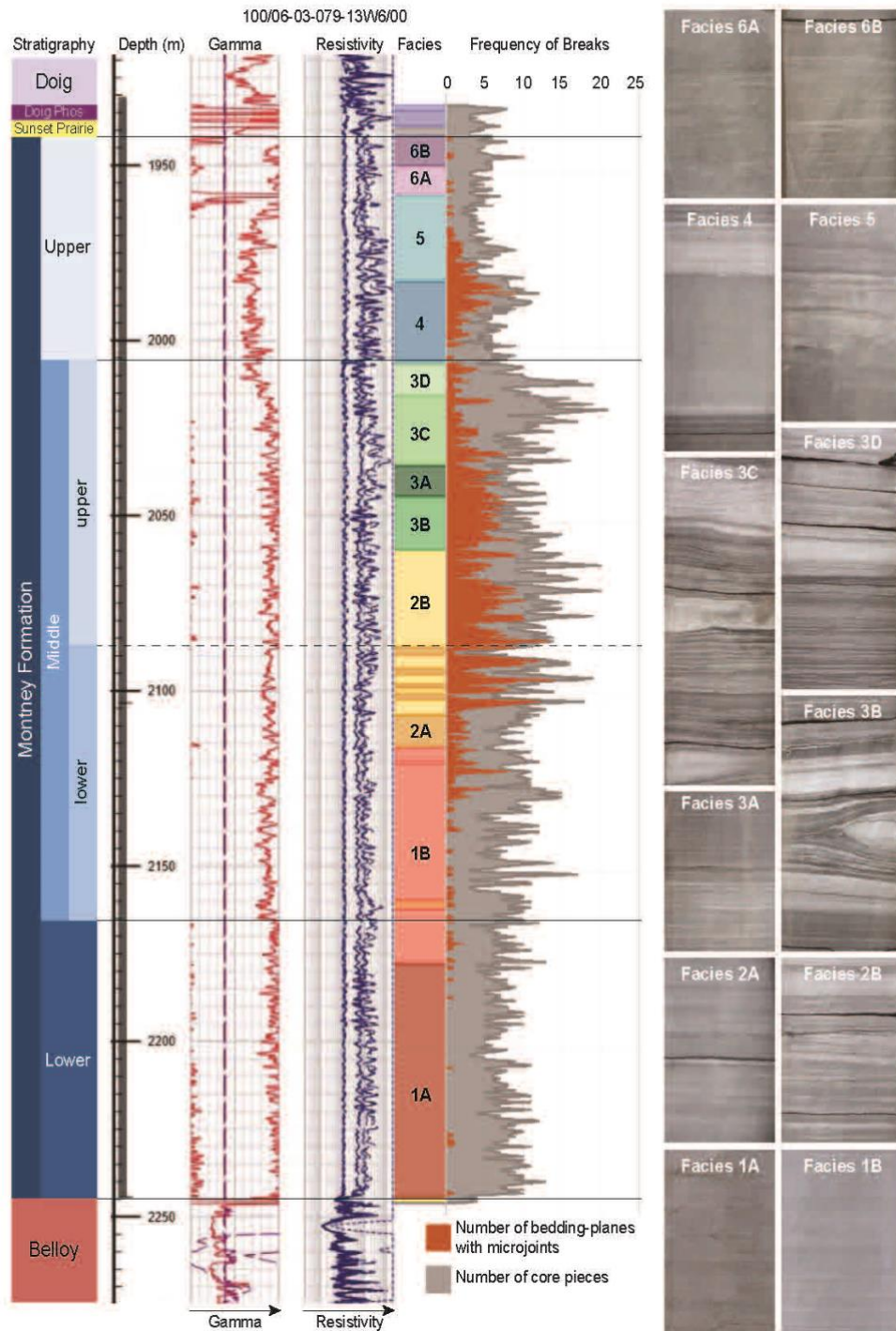


**Figure 10.** Detailed log for 06-03-79-13W6 and photos of typical facies appearance.

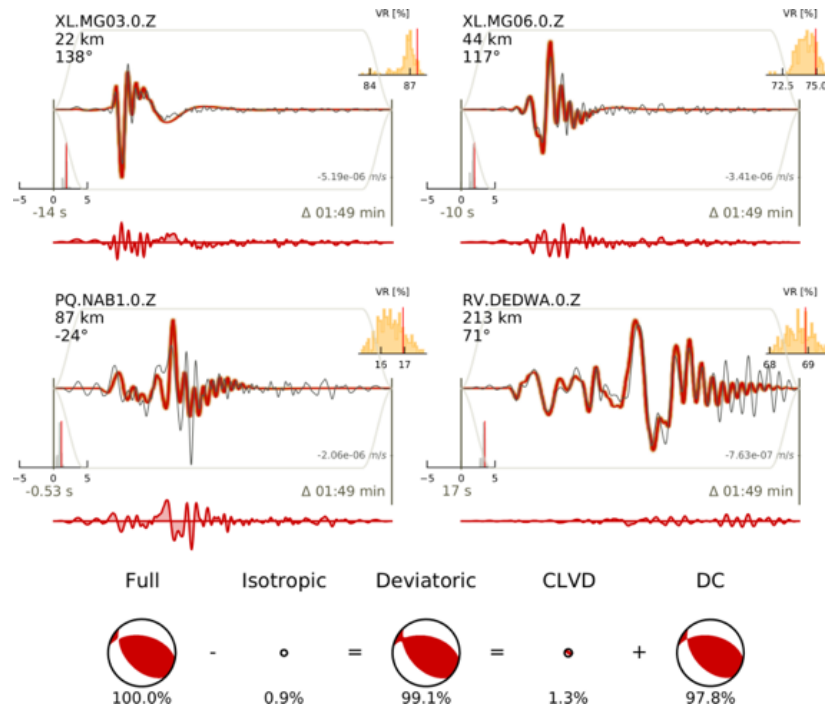


**Figure 11.** Waveform fits, and moment tensor decomposition for the ML 4.2 November 30, 2018 event in the Septimus area using a Bayesian source inversion using the BEAT software (Vasyura-Bathke et al., 2020). Waveform fits are shown in the top 4 panels for vertical components of 4 seismic stations. Each panel shows observed data (solid black line), the best fit data prediction (solid red line), and two inserts with probability distributions. The top-right insert shows the range of percent variance reductions (VR) achieved by predictions for the complete posterior ensemble of models. Larger VR values indicate better fit to the data. The bottom-left insert shows marginal distributions of time-shift station corrections. These corrections are applied to account for errors in origin time and errors due to the presence of 3D velocity effects while the Green functions are based on a 1D velocity model.

### *Temporal variations in site response*

Site response is a measure of ground-motion amplification. Sites with thick, unconsolidated layer above bedrock are generally prone to higher levels of amplification (Monahan, 2018). Amplification often occurs primarily in relatively narrow frequency band, which is important for hazard analysis in cases where the natural ground-motion amplification overlaps with resonances of structures such as buildings and infrastructure (Igweze, 2021). Previous studies of the site response in the KSMMA (Monahan, 2018; 2019; 2020) have focused on time-invariant site classification based on shallow geological structure. The potential for temporal variations in site response has not previously been considered. This research component uses a different approach, based on the spectral analysis of micro-tremors. This approach computes the fundamental-mode frequency of site-response

spectrum using the horizontal to vertical spectra ratio (HVSR) method (Nakamura, 1989). Details of the analysis are provided by Igweze (2021).

Data used in this study were retrieved from the KSMMA array and processed using the HVSRPY python package (Vantassel, 2020). For each station, and for every day over a 365-day period, the HVSR curve was calculated by dividing the spectral amplitudes of the total horizontal component, obtained from the vectorial amplitude of the spectra for the east-west and north-south components (Igweze, 2021), by the spectrum of the vertical component, without removing any data segments (e.g., earthquakes). The shape of the HVSR curve is controlled by S-wave resonance in the subsurface. In general, HVSR spectra show distinct frequency peaks (Figure 12) that are consistent with local geological setting and previous time-averaged shear-wave velocity to 30 m depth, also known as Vs30 reports. Secondary peaks are also evident that become more, or less, prominent throughout the year and sometimes become the dominant spectral peak.

Figure 13 shows representative examples of variation, or lack thereof, in the fundamental HVSR frequency ( $f_0$ ) versus time (plots for every station are given by Igweze, 2021). The fundamental frequency is automatically selected by HVSRPY as the highest spectral peak based on the median spectrum based on hourly spectra (Figure 12). In some cases, HVSR spectra are multimodal, reflect complex resonances from multiple near-surface layers. Abrupt changes in the fundamental-mode frequency can occur in cases multiple spectral peaks exist with temporally varying amplitude. Igweze (2021) showed that gradual change in the relative amplitude of two spectral peaks can result in an abrupt change in  $f_0$ , when the ordering of the highest peak changes (i.e., a secondary peak becomes the primary peak). Furthermore, Igweze's (2021) results show that when seasonal warming or cooling occurred during 2020, this corresponds, in some cases, with an abrupt change in the fundamental mode frequency (Figure 13c). Igweze (2021) hypothesized that changes in the relative prominence of different spectral peaks is driven by seasonal variations in water saturation and/or frozen ground conditions. Since the details of the spectrum (i.e., the peak frequencies) depend on the local site geology, there is no expectation that the temperature modulation of the peaks would produce a similar shift (i.e., decrease or increase) at every station.

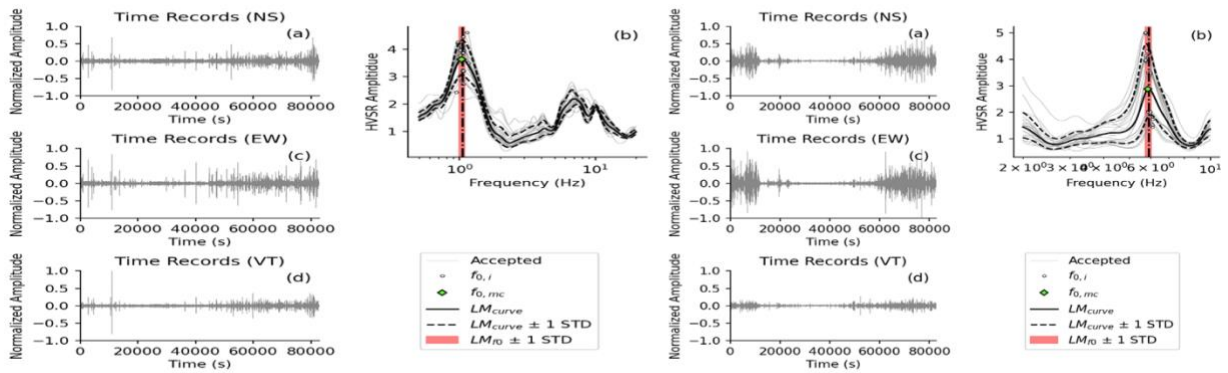


**Figure 12.** Representative examples of 1-day HVSR amplitude plots for station KSM03 (left) and KSM04 (right) on August 24 and July 24, 2020, respectively. Solid black line shows the median HVSR curve, light gray curves show one-hour plots, and dashed lines show 95% confidence region. Green dot indicates the peak resonant frequency,  $f_0$ . Red block shows standard deviation of the peak resonant frequency. The spectrum for KSM03 (left) shows a secondary peak at ~ 6.5 Hz. HVSR plots for all stations can be found in Igweze (2021).

Station	Evidence for seasonal variability	Average HVSR Resonant Frequency $f_0$ [Hz]	Calculated $f_0$ using model from Monahan (2020) [Hz]
KSM01	Spring and Fall	5.34	4.00
KSM02	Spring	2.10	2.70
KSM03	No	3.08	2.04
KSM04	No	5.60	4.17
KSM05	Spring	6.86	5.00
KSM06	No	7.90	11.10
KSM07	No	3.46	4.30
KSM08	No	2.99	2.50
KSM09	Early/late Summer	2.90	3.50
KSM10	No	2.83	2.70
KSM11	Spring and Fall	3.64	4.50
KSM12	No	10.34	3.22
KSM13	Spring and Fall	4.64	2.50

**Table 2.** Average HVSR resonant frequency for each station compared with resonant frequency calculated using the nearest measurement from the Monahan et al. (2020), using the formula  $f_0 = V_s/4h$  (see text for details). Stations that show evidence for seasonal change, similar to the example in Figure 13c, are indicated.

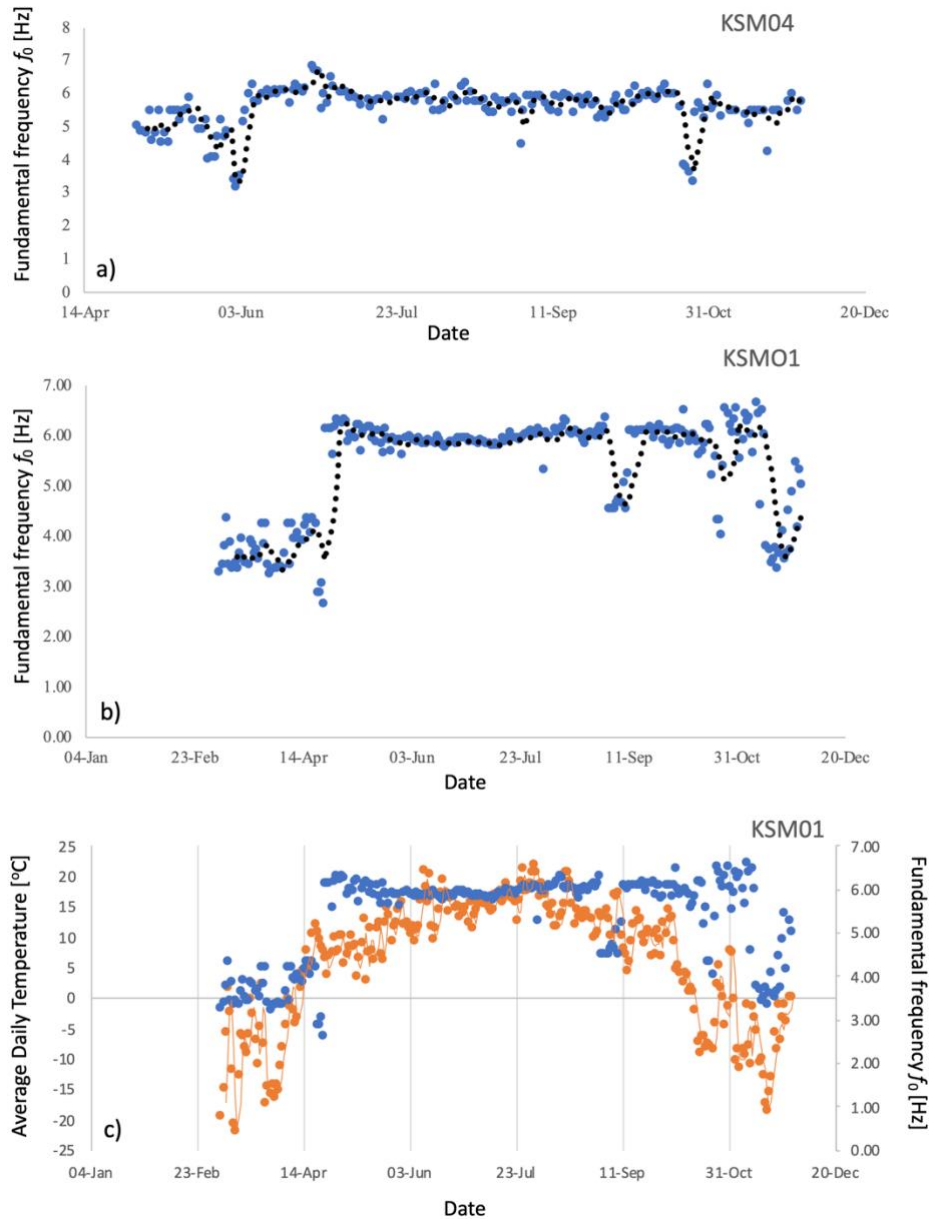


**Figure 13.** Representative examples of median daily HVSR fundamental frequency, picked automatically by HVSRPY software, versus date during 2020. Black dotted lines show 8-day moving average trend. a) Station KSM04 shows consistent results throughout the year with no evidence for seasonal variability. b) Station KSM01 shows a sudden increase in fundamental frequency in the Spring and a drop in late Fall (with a smaller reduction for a few weeks in early Fall). c) Overlay of fundamental frequency from (b), shown by the blue dots, with the daily average temperature in Fort St. John, BC, shown by the orange dots with a solid orange curve. Temperature data is provided by Environment Canada and was downloaded from <https://ftstjohn.weatherstats.ca>.

Table 2 shows the annual average fundamental HVSR resonant frequency ( $f_0$ ) for all EO broadband seismograph stations in the KSMMA compared with calculated  $f_0$  obtained from the closest location reported by Monahan et al. (2020). The calculated value of  $f_0$  represents the expected HVSR resonant frequency for a single layer over a half space, given by (Igweze, 2021)

$$f_0 = \frac{V_s}{4h} ,$$

where  $V_s$  and  $h$  are the shear-wave velocity and thickness, respectively, of the shallowest layer in the model. There are similarities and differences between the observed and calculated models that are summarized in Table 2, likely resulting from differences between the simple model (one layer over a half space) and the realistic scenario (multiple shallow layers). Further research is needed to better understand how temporal variations in HVSR site response reflect specific changes in near-surface conditions, these preliminary results show that site response is not strictly time invariant. This could have ramifications for seasonal variability in how ground shaking is felt by local residents.

### *Relative Quiescence in the KSMMA – April to September 2020*

Due to the global pandemic of COVID-19, the year 2020 offered unique insights into the detection of seismicity which may usually go unnoticed due to other factors such as ongoing anthropogenic activity or noise. For example, within the KSMMA seismicity has always been thought to be temporally and spatially correlated with ongoing unconventional resource exploration, with very little natural seismicity (e.g., Lamontagne et al., 2008). However, with the suspension of such operations due to the subsequent downturn in the economic market and fall in energy stock prices as a result of COVID-19, we were able to detect seismicity that cannot be directly attributed to such activities for the first time. In part, this was due to the reduction in seismic ambient noise in the KSMMA (and around the world) as shown in Figure 14, which has been correlated to a decrease in the amount people are moving due to lockdown measures (e.g., Lecocq et al., 2020).

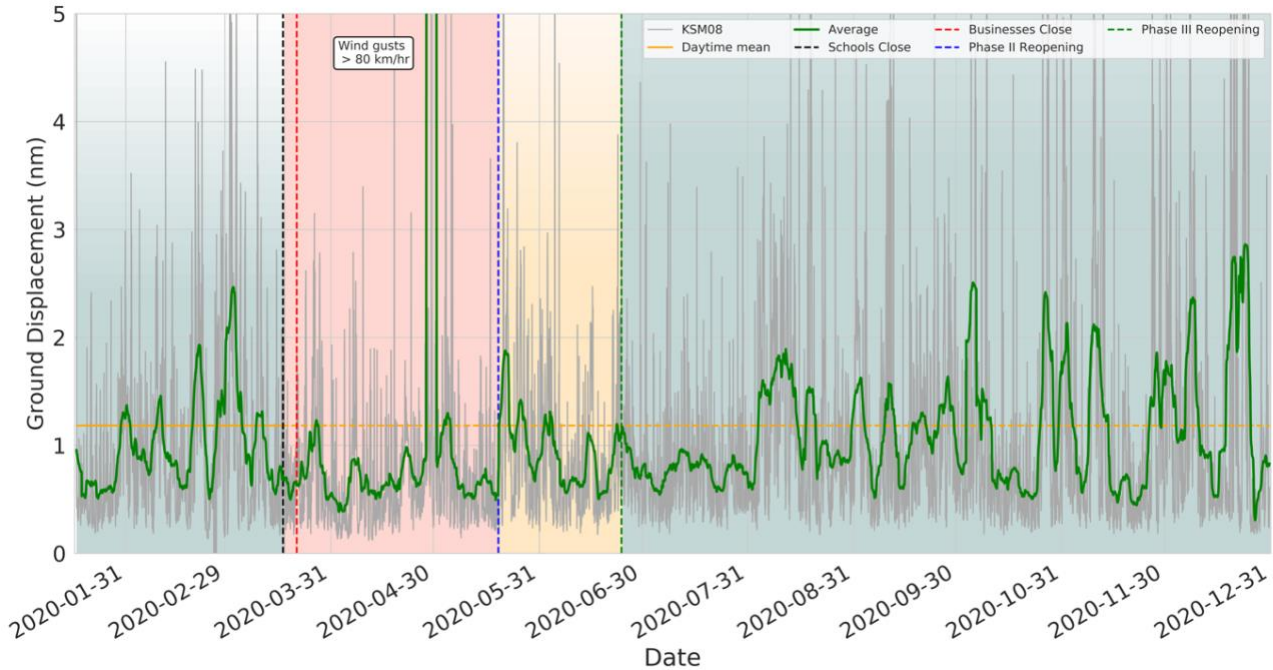


**Figure 14.** Filtered (4 – 14 Hz) ambient seismic noise displayed as displacement at station KSM08, vertical component. The average rolling mean (window size = 72 hours) of ground displacement is shown in green. Background colours represent different lockdown scenarios in British Columbia.

Seismic ambient noise can be estimated at a single station by calculating the probabilistic power spectral density (PPSD) and converting to displacement. In order to capture anthropogenic noise, we use the frequency band of 4 – 14 Hz since cultural noise typically manifests at high frequencies (> 1–10 Hz, McNamara and Buland, 2004). A reduction in seismic noise (and consequently in ground motion) can be observed for the KSMMA during the COVID-19 lockdown (Figure 14). Heightened ground motions are observed from January to March 2020, thought to be associated not only with the movement of people throughout the area, but also to the ongoing unconventional resource development. A significant drop in this average ground motion is first observed in late March, following government enforced lockdowns in British Columbia, which seriously affected the stock of many companies operating in this area, and led to the subsequent suspension of operations (throughout the time period coloured red). With each easing of the lockdown rules, and the increasing price and demand for unconventional resources as the economy recovered, we see a gradual increase in the average ground displacement once more (moving from red, to yellow, to green background colours in Figure 14).

A total of 4,268 seismic events were detected within the KSMMA using the EO network from 1 January 2020 to 1 April 2020 (prior to lockdown scenarios in British Columbia in 2020), compared with 3,176 events from 6 August 2020 to 1 January 2021, once most lockdowns had been lifted or partially lifted (Salvage and Eaton, 2021). However, from 1 April to 6 August 2020, only 389 events were detected within the KSMMA, with an average of ~5 events per day (Figure 15a). The timing of seismic events was taken from the catalogue provided by Nanometrics. Events are detected from incoming continuous seismicity using an STA/LTA algorithm, followed by a template matching procedure. Phase arrivals are then determined using a machine-learning algorithm that uses historical seismicity as a training database. Hypocentre locations were determined using NonLinLoc (Lomax et al., 2009), a grid-search algorithm, followed by relocations using the double difference travel-time of events determined using HypoDD (Waldhauser and Ellsworth, 2000). We used a 1-D velocity model specifically calibrated for the KSMMA using formation tops and compression and shear sonic logs, from the BC Oil and Gas Commission (Salvage et al., 2021).

Local magnitudes were calculated using the updated formula of Babaie Mahani and Kao (2020), which has been calibrated for the KSMMA. Magnitudes remain fairly constant between  $\sim M_L 0$  and  $\sim M_L 1$ ; the largest recorded event during this period was  $M_L 1.23$  (Figure 15a). The frequency index (FI) of waveforms (Buurman and West, 2010) determines the amount of high-to-low frequency energy within each detected waveform. Therefore, a  $FI > 0$  indicates the waveform is dominated by high-frequency energy and a  $FI < 0$  indicates one dominated by low-frequency energy. All waveforms detected during the period of relative quiescence appear to be dominated by low-frequency energy, which may indicate processes involving fluid (e.g., Lahr et al., 1994) or aseismic slip (Zoback et al., 2012) may play a pivotal role in the generation of this seismicity. Spatially, seismicity falls within the recognized corridor of seismicity within the KSMMA (orientated NW-SE) where seismicity has previously been detected (Figure 15b). Focal depths appear to vary more than when seismicity solely attributed to hydraulic fracturing is occurring (for example, see seismicity close to Farmington in February 2021, this report).

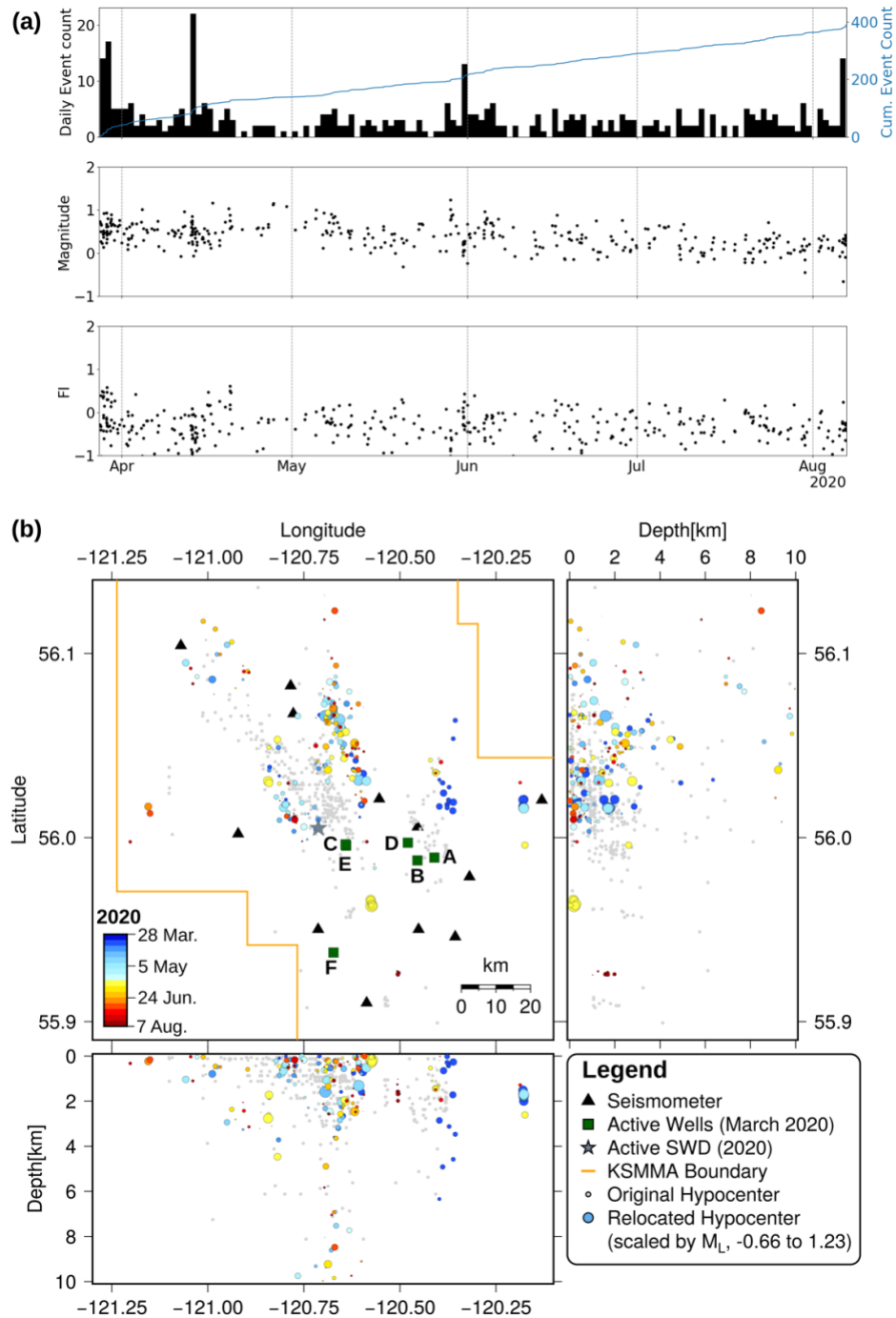


**Figure 15.** a) Temporal evolution of seismicity during period of relative quiescence from April to August 2020. Magnitudes were determined using the formula of Babaie-Mahani and Kao (2020). The temporal evolution for the full time window is shown in Figure 5. b) Spatial evolution of seismicity showing original hypocenters and relocated hypocenters, coloured by time and scaled by magnitude. Active wells in March 2020 are shown as green squares (labelled from most recently active (A) to least recently active (F)).

The seismicity detected during this unusual phase of relative quiescence has been interpreted as “latent seismicity”, i.e., seismicity that continues to occur after a relatively long time following a primary activation processes, but which has no obvious trigger (e.g. hydraulic fracturing operations). Some of this seismicity may be attributable to natural seismicity, however given that natural seismicity was difficult to detect prior to the introduction of unconventional resource development in the area because of a limited seismic recording network, it is difficult to determine the rates of background natural seismicity. Some of the detected seismicity is thought to relate to a single operational hydraulic fracturing well and ongoing produced or salt-water disposal throughout the period of relative quiescence, and some may be the result of dynamic triggering from more distant events. However, ~65% of the detected seismicity cannot be attributed to any of these scenarios (Salvage and Eaton, 2021). Possible causative factors include ongoing isostatic adjustment from the last glacial maximum (e.g., Steffen et al., 2014) and/or ongoing compressive stress from the southwest (Kao et al., 2018), oblique to the heavily faulted Fort St. John graben complex.

### *Seismicity near Farmington – February to March 2021*

Seismicity at the beginning of 2021 was generally low, with an average of 5 – 10 events being detected in the KSMMA per day in January. Events in February to March 2021 are generally located within a corridor orientated NW-SE, as has previously been seen in this area (e.g., Salvage et al., 2020). At the end of February 2021, a short sequency of seismicity began south of Farmington, where almost 650 events were detected between 23<sup>rd</sup> February and 5<sup>th</sup> March.

Figure 16 shows the temporal evolution of seismicity from 23<sup>rd</sup> February 2021 onwards. Events appear to be temporally clustered, with the majority of the events occurring between 24<sup>th</sup> February 12:00 UTC and 26<sup>th</sup> February 00:00 UTC. Hourly event rates peaked on 25<sup>th</sup> February from 00:00 to 12:00 UTC. Two shorter swarms with far less events occurred from 28<sup>th</sup> February to 1<sup>st</sup> March, and on 4<sup>th</sup> March 2021. The first of these swarms included the largest magnitude event in the sequence: a  $M_L$  2.03 (28<sup>th</sup> February, 23:50 UTC at a depth of 1.74 km). Recorded magnitudes throughout this sequence have ranged from  $M_L$  -0.32 to  $M_L$  2.03 (Babaie-Mahani and Kao, 2020  $M_L$  calculation), in a typical swarm-like sequence with limited evidence of a mainshock-aftershock type decay. Detected seismicity also appears clustered spatially (Figure 17), close to a known active hydraulic fracturing well in the

area. Events depict linear features in map view and are highly clustered at depth, although the absolute depth of these events requires further investigation as noted above.

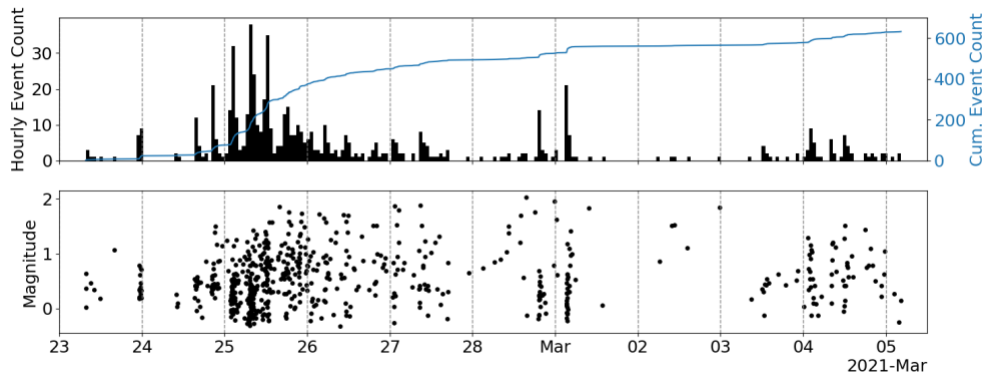


**Figure 16.** Temporal evolution of seismicity detected within the KSMMA near Farmington, British Columbia from 23<sup>rd</sup> February to 5<sup>th</sup> March 2021. Magnitudes were calculated using the scale of Babaie Mahani and Kao (2020).

The frequency-magnitude distribution of these events is shown in Figure 18 ( $n=632$ ). The magnitude of completeness, calculated using the maximum-curvature method of Wiemer and Wyss (2000), was estimated to be 0.38, which is slightly higher than the estimated  $M_c$  for all the detected seismicity from January 2020 to March 2021 ( $M_c \sim 0.17$ ). This in part reflects the number of events within each distribution (over 9500 events were used for calculating the  $M_c$  for 2020/2021). The estimated  $b$ -value for the detected sequence near Farmington is  $\sim 1.42$ , which is lower than that estimated value for 2020/2021 ( $b$ -value  $\sim 1.74$ ), suggesting an abundance of lower magnitude events in this sequence.

### *Updated Structural Database*

This component of the project is aimed at compiling an updated structural database for in the Western Canada, putting emphasis of the fault distribution in the KSMMA. Currently existing fault databases are very often incomplete and/or indicate erroneous locations of the structures due to errors related to digitization from published figures. It is therefore necessary to review the available datasets, check their correctness as well as improve the completeness of the fault structures within the KSMMA region. The KSMMA is contained within the Peace River Arch, characterized by the variety of structural features. Substantial subsidence and associated faulting resulted in the formation of the multiple horst and graben blocks, including the Fort St. John Graben, part of the Dawson Creek Graben Complex (DCGC) (Barclay et al., 1990). Although multiple previous studies investigated the tectonic

history and location of the major faults in the area (Barclay et al. 1990; Richards et al., 1994; Mei et al., 2009; Furlong et al., 2020), the results are not consistent. Multiple features are identified in the wrong position or are mislabeled (Mei, 2009).

We have investigated published fault databases and performed an analysis of the geophysical data including 2D seismic and microseismicity to compile a high-quality catalogue of faults within the KSMMA region. We also used publicly available 2D seismic dataset obtained within the LITHOPROBE research program (Clowes, 2010). Specifically, part of the LITHOPROBE transect used in this study includes the Peace River Arch Industry Seismic Experiment (PRAISE) subset. PRAISE consisted of over 600 km reflection seismic lines and was recorded in 1994. The dataset was previously used to identify the major fault structures within the Peace River Arch region (Eaton et al., 1999). This study focuses on the several lines from this project (11a-14bc. Fig. 19), which are contained within the study region.

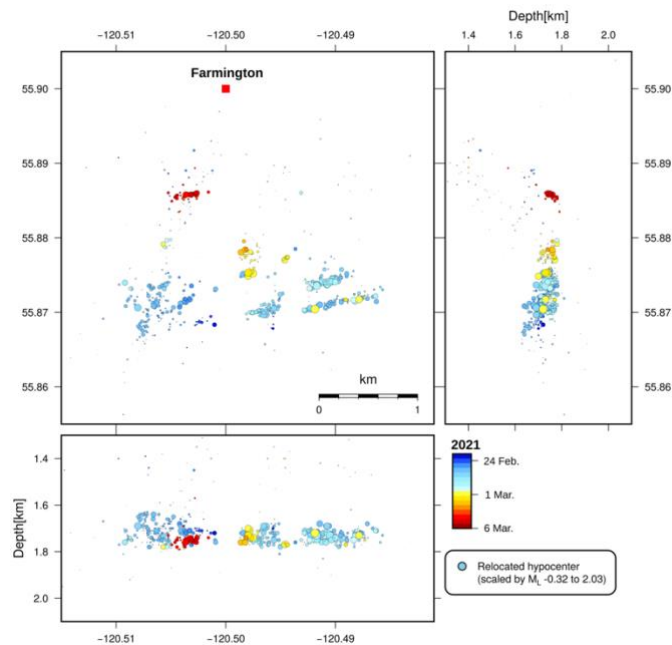


**Figure 17.** Spatial evolution of seismicity in February and March 2021 close to Farmington, British Columbia. In map view, events depict clear linear features. Events are closely clustered in depth between 1.6 km and 1.8 km, likely related to the Montney target formation.

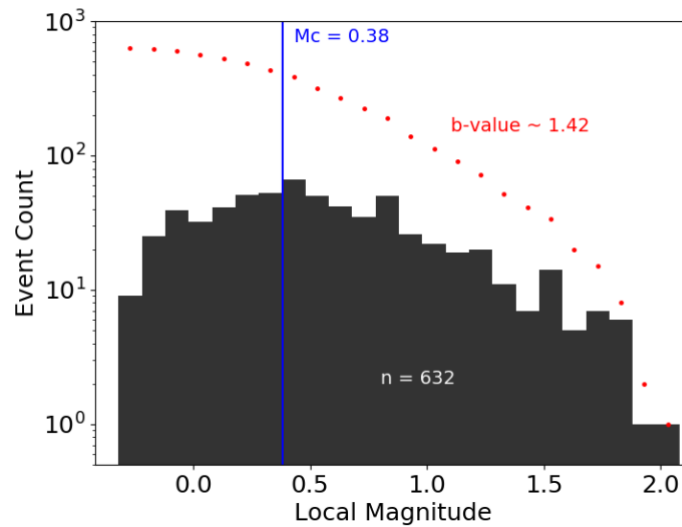


**Figure 18.** Frequency-Magnitude distribution of events detected near Farmington from 23<sup>rd</sup> February to 5<sup>th</sup> March 2021 ( $n=632$ , Babaie Mahani and Kao, 2020  $M_L$  calculation). The estimated magnitude of completeness ( $M_c$ ) is 0.38, and the estimated  $b$ -value is 1.42

In addition to seismic and well data, catalogues of microseismic events are being used to constrain possible fault locations. Microseismicity can be successfully used to infer the locations of faults, where seismic data is not available, or the vertical offset of the fault is below the detection threshold (Eyre et al, 2019a, Skoumal et al., 2019). Based on our initial interpretation, several major fault structures can be identified on the seismic sections. Next steps of this study include the detailed analysis to associate interpreted fault with the structures published in the literature. Moreover, we will investigate in details the induced seismicity clusters detected using the KSMMA monitoring array. The final step in this process will include compilation of all the results into a database containing shapefiles.

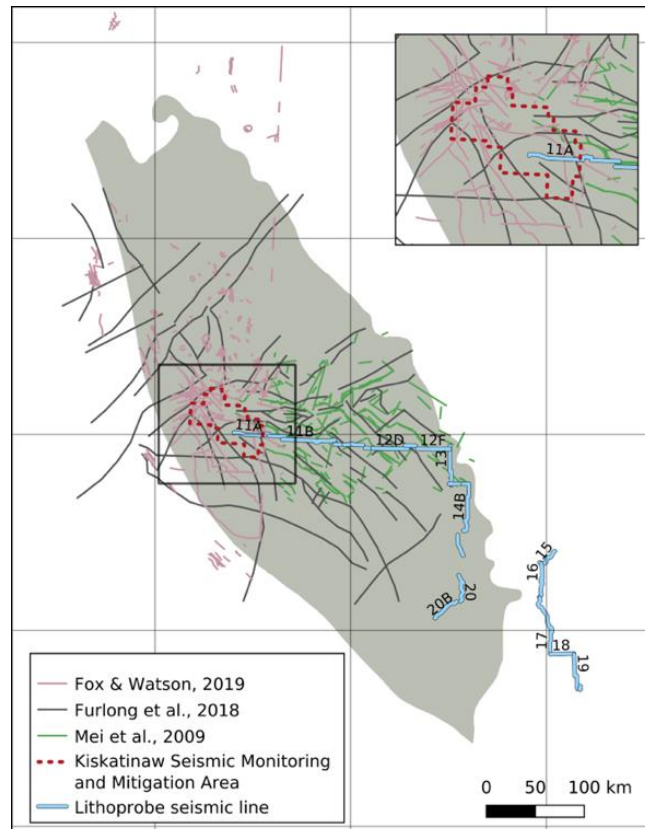


**Figure 19.** Map of faults, compiled from the literature grouped by publication. Shaded area shows the Montney play. Location of KSMMA monitoring region and LITHOPROBE lines are outlined by the red dashed lines and wide blue lines, respectively. We caution that the depth extent of these faults is the subject of ongoing investigation, as not all of these may be relevant for the Montney play that is the focus of this investigation.

## Summary and Future Work

This research project is managed by the University of Calgary and has involved the installation and operation of a dense array of sensors within the Kiskatinaw Seismic Monitoring and Mitigation Area (KSMMA), comprised of 15 stations (13 broadband seismometers and 2 accelerometers). Nanometrics, an experienced service provider, was contracted to install and operate the dense array, including troubleshooting, cloud-based data acquisition and archiving systems. The operation of this dense array has allowed detection of numerous small events that help to characterize faults as well as mapping of ground shaking in more detail than would otherwise be possible. Using these data, a comprehensive seismicity catalogue for the period 2020/01/22 to 2021/03/31 accompanies this report, containing 9,740 events in the local magnitude range  $-0.73 \leq M_L \leq 3.41$ . In addition to this seismicity

catalogue, continuous waveform data have been made available to all researchers and participating industry sponsors. Following a rolling embargo period of 91 days, all data have been released through the Incorporated Research Institutions for Seismology (IRIS), a widely used international archival resource for seismological data.

The data acquired for this project is supporting a vigorous research program at the University of Calgary that will continue beyond the timeframe of the current Geoscience BC project through a grant from NSERC's Alliance program. As part of the current project, research themes at the University of Calgary include the following: 1) generation of empirical shakemaps using all available public real-time stations, a well-established approach in earthquake seismology that enables rapid mapping and presentation of peak ground acceleration (PGA) and ground-shaking intensity; 2) geomechanical analysis aimed at understanding the possible role of lateral pore-pressure gradients on fault rupture; 3) probabilistic determination of earthquake source mechanisms using BEAT software; 4) development and refinement of a regional geological framework; 5) calculation and interpretation of temporal variations in local site response using the HVSr method; 6) detailed analysis of spatiotemporal patterns of seismicity; 7) progress in developing an updated regional fault database for the Western Canada Sedimentary Basin, constrained by well and seismic data; 8) detailed analysis of temporal changes in  $b$ -value, as well as source spectral characteristics, as a potential indicator of transition from normal hydraulic fracturing operations to fault activation (Maxwell, 2009; Eaton and Maghsoudi, 2015). Future work may also include calculation of Peak Ground Velocity (PGV), Peak Ground Displacement (PGD), and Peak Spectral Acceleration (PSA) at several frequencies, which could provide an excellent opportunity to calibrate the existing Ground Motion Prediction Equations (GMPEs) for the region, or to develop new ones.

The results presented in this report support a number of preliminary conclusions. First, it is evident that the availability of real-time continuous data from a dense array of stations could be used to generate automatic shakemaps, which would be very helpful to better understand and respond to spatially variable ground shaking due to induced events. Here, PGA values were computed mainly using broadband seismometers rather than accelerometers. For the relatively weak ground shaking that occurred during the timeframe of this project, this approach seems to be effective, since consistent results were obtained in most cases where seismometers and accelerometers were co-located. In the case of strong ground motion, accelerometers have the advantage that they generally would not go off

scale except under extreme circumstances. One finding of this work is that, for a given magnitude level, PGA measured in this study within the Farmington area appears to be systematically greater than PGA values reported in the Septimus and Graham areas; however, more work is needed to evaluate the robustness of this finding.

Other preliminary conclusions from ongoing research include:

1. Spatial relationships between mapped faults and areas of induced seismicity suggest that potential seismogenic structures (i.e., some, but not all, inactive geological faults) can be identified and mapped. This information is currently being used to improve the analysis of geological susceptibility to induced seismicity within structural corridors, including subseismic faults (those whose throw is too small to be detected using seismic methods). In particular, it appears that areas of high seismicity rate do not correlate spatially with locations of the largest events (M 3-4+).
2. Probabilistic studies of earthquake mechanisms enable rigorous quantification of uncertainty, leading to more robust moment-tensor inversion results. This approach also holds promise for estimating source-time functions, which may reveal both fast (dynamic rupture) and slow (creep) fault processes.
3. Ongoing work to compile and map existing faults can be used to test previous interpretations that pre-existing faults, which form part of the Carboniferous-age Fort St. John graben complex, bound Montney reservoir compartments with distinct pore-pressure levels.
4. Microtremor analysis using horizontal-vertical spectral ratios (HVSR) has been analyzed in conjunction with complementary Vs30 measurements (Monahan et al., 2018; 2019; 2020) as a way to quantify earthquake site response (Igweze, 2021). Advantages of the HVSR approach is that it reveals resonant behaviour of soils that could be significant for structural response and perception of ground motion. In addition, the HVSR approach allows temporal variations in site response to be characterized. Analysis of 12 months of data from KSM stations indicates that HVSR response at many stations is multi-modal, consistent with multi-layered near-surface velocity structural, and temporal variability may be driven by changes in the relative strength of different spectral peaks.

5. Latent seismicity persisted throughout the COVID lockdown period (April – August 2020). Seismicity levels were lower than during periods of normal industrial activity, but magnitude-frequency recurrence statistics (Salvage and Eaton, 2021) indicate that seismicity levels during this period were too high to be attributed entirely to natural seismicity. This suggests that the seismicity response to fluid injection may include persistent swarm-like behaviour, or interaction between hydraulic fracturing and produced or salt-water disposal that continued during the lockdown.

Future work for the regional geological framework component of this project will include investigating and logging core across the KSSMA region. Cores will be selected based on length, stratigraphic distribution, and proximity to induced seismicity event locations. Other core datasets, (e.g. mineralogy from XRD, TOC, geomechanics) will be further integrated into the dataset to better understand lateral and vertical heterogeneities within the Montney Formation. In terms of the geomechanical analysis component of this project, future work will include discrete-element numerical simulation of the effects of a strong lateral pore pressure gradient on fault rupture behaviour. In terms of the Bayesian moment-tensor inversion component of this project, ongoing studies will refine the methodology and apply this approach to additional events. With respect to the fault database component of the project, the collection of additional data for fault identification and validation is currently underway. Opportunities to leverage and to enhance public communication and indigenous relations are available through the NSERC-funded CREATE-REDEVELOP (Responsible Development of Low Permeability Hydrocarbon Resources) national program that is led by the University of Calgary.

In summary, this project has enabled significantly enhanced seismicity and ground-motion monitoring, in near real-time, within an area of known sensitivity to induced seismicity. This work provides direct benefits for the regulator, industry, and ultimately the public through the release of open-access data and analysis. Substantial, publicly accessible documentation of research results is being created through conference presentations, student thesis projects and peer-reviewed scientific publications.

## Acknowledgements

The authors wish thank Geoscience BC for funding this project. They also wish to thank the industry partners whose collaboration enabled the installation of this network. They would like to thank ARC Resources Ltd., Canadian Natural Resources Limited and the Natural Sciences and Engineering Research Council of Canada for providing further funding for this project. Nanometrics Seismic Monitoring Services is gratefully acknowledged for their contribution to this project, including the installation and maintenance of stations, and near real-time analysis of incoming seismicity. The authors would like to thank those at the Incorporated Research Institutions for Seismology (IRIS) for hosting the data and facilitating collaboration. They would especially like to thank J. Hogan at Nanometrics, who facilitated the successful upload of data to IRIS, and A. Baig at Nanometrics for review of an earlier version of this manuscript. Also, thanks go to H. Vasyura-Bathke at the University of Potsdam/GFZ German Research Centre for Geosciences for their support in determining centroid moment tensor parameters. We are grateful for access to data from the XL network ([https://www.fdsn.org/networks/detail/XL\\_2017/](https://www.fdsn.org/networks/detail/XL_2017/)) for the moment tensor inversion. Finally, they would like to thank S. Venables and M. Gaucher at the BC Oil and Gas Commission for their continued support and invaluable knowledge that the authors have often called upon.

## References

- Aki K. (1965). Maximum likelihood estimate of  $b$  in the formula  $\log N = a - bM$  and its confidence limits. *Bulletin of the Earthquake Research Institute of Tokyo University*, 43, 237-239.
- Babaie Mahani, A. B., and Kao, H. (2018). Ground motion from M 1.5 to 3.8 induced earthquakes at hypocentral distance < 45 km in the Montney play of northeast British Columbia, Canada. *Seismological Research Letters*, 89(1), 22-34.
- Babaie Mahani, A. B., and Kao, H. (2019). Accurate determination of local magnitude for earthquakes in the western Canada sedimentary basin. *Seismological Research Letters*, 90(1), 203-211.
- Babaie Mahani, A. and Kao, H. (2020): Determination of local magnitude for induced earthquakes in the Western Canada Sedimentary Basin: an update; *CSEG Recorder*, 45(2).
- Bao, X., & Eaton, D. W. (2016). Fault activation by hydraulic fracturing in western Canada. *Science*, 354(6318), 1406-1409.
- Eaton, D.W. (2018): *Passive seismic monitoring of induced seismicity: fundamental principles and application to energy technologies*. Cambridge University Press.

- Barclay, J.E., Krause, F.F., Campbell, R.I., and Utting, J. (1990). Dynamic casting and growth faulting: Dawson Creek Graben Complex, Carboniferous-Permian Peace River Embayment, Western Canada. In: *Geology of the Peace River Arch*. S.C. O'Connell and J.S. Bell, (eds.). *Bulletin of Canadian Petroleum Geology*, v. 38A, 115-145.
- BC Oil and Gas Commission (BCOGC) (2016): *Industry Bulletin 2016-19*, <https://www.bcogc.ca/node/13257/download>.
- BC Oil and Gas Commission (2018): *Order 18-90-001 (amendment #1) – Kiskatinaw Seismic Monitoring and Mitigation Area Special Project Order*; BC Oil and Gas Commission.
- Bustin, A. and Bustin, R. (2017): *Geoscience BC Summary of Activities 2016*, Geoscience BC, Report 2017-1.
- Buurman, H. and West, M.E. (2010). Seismic precursors to volcanic explosions during the 2006 eruption of Augustine Volcano. *The 2006 eruption of Augustine volcano, Alaska*, Edited by Power, J. A., Coombs, M. L., and Freymueller, J., U.S. Geological Survey Professional Paper 1769, 41-57.
- Clowes, R. M. (2010). Initiation, development, and benefits of Lithoprobe—shaping the direction of Earth science research in Canada and beyond. *Canadian Journal of Earth Sciences*, 47(4), 291-314.
- Crombez, V., Rohais, S., Baudin, F., & Euzen, T. (2016). Facies, well-log patterns, geometries and sequence stratigraphy of a wave-dominated margin: insight from the Montney Formation (Alberta, British Columbia, Canada). *Bulletin of Canadian Petroleum Geology*, 64(4), 516–537.
- Crombez, V., Baudin, F., Rohais, S., Riquier, L., Euzen, T., Pauthier, S., Ducros, M., Caron, B., & Vaisblat, N. (2017). Basin scale distribution of organic matter in marine fine-grained sedimentary rocks: Insight from sequence stratigraphy and multi-proxies analysis in the Montney and Doig formations. *Marine and Petroleum Geology*, 83, 382–401.
- Davies, G., Hume, D., Fox, A., Haysom, S., Nevokshonoff, G., & Reinmiller, R. (2014). Core-based structural fabrics in mudstones of the WCSB: 'PSF' and cleavage, In *Unconventional Resources Technology Conference*.
- Davies, G. R., Watson, N., Moslow, T. F., & MacEachern, J. A. (2018). Regional subdivisions, sequences, correlations and facies relationships of the Lower Triassic Montney Formation, west-central Alberta to northeastern British Columbia, Canada - with emphasis on role of paleostructure. *Bulletin of Canadian Petroleum Geology*, 66(1), 23–92.
- De Barros, L., Cappa, F., Guglielmi, Y., Duboeuf, L., & Grasso, J. R. (2019). Energy of injection-induced seismicity predicted from in-situ experiments. *Scientific Reports*, 9(1), 1-11.
- Eaton, D.W. (2018): *Passive seismic monitoring of induced seismicity: fundamental principles and application to energy technologies*. Cambridge University Press.
- Eaton, D. W., Ross, G. M., & Hope, J. (1999). The rise and fall of a cratonic arch: A regional seismic perspective on the Peace River Arch, Alberta. *Bulletin of Canadian Petroleum Geology*, 47(4), 346-361.
- Eaton, D. W. and Maghsoudi, S. (2015). 2b... or not 2b? Interpreting magnitude distributions from microseismic catalogs. *First Break*, 33(10).

- Eaton, D., Mahani, A., Salvage, R., Kao, H. and van der Baan, M. (2019): Proceedings of the CSPG 2019 Gussow Conference.
- El-Isa, Z.H. and Eaton, D.W., 2014. Spatiotemporal variations in the  $b$ -value of earthquake magnitude–frequency distributions: Classification and causes. *Tectonophysics*, 615, pp.1-11.
- Eyre T.S., Eaton D. W., Zecevic M., D’Amico, D., Kolos, D. (2019a). Microseismicity reveals fault activation before  $M_w$  4.1 hydraulic-fracturing induced earthquake, *Geophysical Journal International*, 218(1), 534–546.
- Eyre, T. S., Eaton, D. W., Garagash, D. I., Zecevic, M., Venieri, M., Weir, R., & Lawton, D. C. (2019b). The role of aseismic slip in hydraulic fracturing–induced seismicity. *Science Advances*, 5(8), eaav7172.
- Fox, A. D. and Watson, N. D. (2019). Induced Seismicity Study in the Kiskatinaw Seismic Monitoring and Mitigation Area, British Columbia. Final report to Geoscience BC.
- Furlong, C. M., Gingras, M. K., & Zonneveld, J. P. (2020). High-resolution sequence stratigraphy of the Middle Triassic Sunset Prairie Formation, Western Canada Sedimentary Basin, north-eastern British Columbia. *The Depositional Record*, 6(2), 383-408.
- Gillen, K., Wood, J., Sharp, L., Grimison, T., & Guerard, B. (2019). Natural and Induced Structural Fabrics in Drillcores from the Montney Formation, Western Canada, In Gussow 2019. CSPG.
- Hutton, L. K., & Boore, D. M. (1987). The ML scale in southern California. *Bulletin of the Seismological Society of America*, 77(6), 2074-2094.
- Igweze, P. (2021). Site response in the Kiskatinaw Seismic Monitoring and Mitigation Area. GOPH 701 report, University of Calgary.
- Kao H., Hyndman R., Jiang Y., Visser R., Smith B., Babaie Mahani A., Leonard L., Ghofrani H. & He J. (2018). Induced seismicity in western Canada linked to tectonic strain rate: Implications for regional seismic hazard. *Geophysical Research Letters*, 45(20), 11-104.
- Lahr, J.C., Chouet, B.A., Stephens, C.D., Power, J.A. and Page, R.A., 1994. Earthquake classification, location, and error analysis in a volcanic environment: Implications for the magmatic system of the 1989–1990 eruptions at Redoubt Volcano, Alaska. *Journal of Volcanology and Geothermal Research*, 62(1-4), 137-151.
- Lamontagne, M., Halchuk, S., Cassidy, J.F. and Rogers, G.C., 2008. Significant Canadian earthquakes of the period 1600–2006. *Seismological Research Letters*, 79(2), 211-223.
- Lecocq, T., Hicks, S.P., Van Noten, K., Van Wijk, K., Koelemeijer, P., De Plaen, R.S., Massin, F., Hillers, G., Anthony, R.E., Apoloner, M.T. and Arroyo-Solórzano, M., 2020. Global quieting of high-frequency seismic noise due to COVID-19 pandemic lockdown measures. *Science*, 369(6509), 1338-1343.
- Lomax, A., Michelini, A., Curtis, A. and Meyers, R.A., 2009. Earthquake location, direct, global-search methods. *Encyclopedia of complexity and systems science*, 5, 2449-2473.
- Maxwell, S.C., Jones, M., Parker, R., Miong, S., Leaney, S., Dorval, D., D’Amico, D., Logel, J., Andersen, E. and Hammermaster, K. (2009): Fault activation during hydraulic fracturing; Society of Exploration Geophysicists, SEG 2009 Annual Meeting, October 25–30, 2009, Houston, Texas, Technical Program Expanded Abstracts, p. 1552– 1556.

- McLellan, P., Anderson, I., Wong, J., & Mostafavi, V. (2014). Geomechanical Characterization of the Farrell Creek Montney Reservoir, Northeast British Columbia, In Geoconvention 2014. CSPG, CSEG, CWLS.
- McNamara, D.E. and Buland, R.P., 2004. Ambient noise levels in the continental United States. *Bulletin of the seismological society of America*, 94(4), 1517-1527.
- Mei, S. (2009). New insights on faults in the Peace River Arch region, northwest Alberta, based on existing well-log data and refined trend surface analysis. *Canadian Journal of Earth Sciences*, 46(1), 41-65.
- Monahan, P.A., Levson, V.M., Hayes, B.J., Dorey, K., Mykula, Y., Brenner, R., Clarke, J., Galambos, B., Candy, C., Krumbiegel, C. and Calderwood, E. (2018): Geoscience BC Report 2018-16.
- Monahan, P. A., Hayes, B. J., Perra, M., Mykula, Y., Clarke, J., Galamboos, B., ... & Oki, U. (2019). Amplification of seismic ground motion in the Fort. St. John–Dawson Creek area, northeastern British Columbia (NTS 093P, 094A). Geoscience BC Summary of Activities, 2020-02
- Monahan, P. A., Hayes, B. J., Perra, M., Mykula, Y., Clarke, J., Gugins, C., ... & Oki, U. (2020). Shear-Wave Velocity Studies of Near-Surface Deposits in the Fort St. John–Dawson Creek Area, Northeastern British Columbia (NTS 093P, 094A).
- Nakamura, Y. (1989). A method for dynamic characteristics estimation of subsurface using microtremor on the ground surface. *Railway Technical Research Institute, Quarterly Reports*, 30(1).
- National Energy Board (2013). <https://www.cer-rec.gc.ca/en/data-analysis/energy-commodities/natural-gas/report/ultimate-potential-montney-formation/the-ultimate-potential-unconventional-petroleum-from-montney-formation-british-columbia-alberta-energy-briefing-note.html>
- Noble, W. S. (2006). What is a support vector machine? *Nature biotechnology*, 24(12), 1565-1567.
- Poulin, A., Weir, R., Eaton, D., Igonin, N., Chen, Y., Lines, L., & Lawton, D. (2019). Focal-time analysis: A new method for stratigraphic depth control of microseismicity and induced seismic events. *Geophysics*, 84(6), KS173-KS182.
- Riazi, N., Eaton, D. W., Aklilu, A., & Poulin, A. (2020). Application of focal-time analysis for improved induced seismicity depth control: A case study from the Montney Formation, British Columbia, Canada. *Geophysics*, 85(6), KS185-KS196.
- Richards, B. C., Barclay, J. E., Osadetz, K. G., Trollope, F. H., & Hartling, A. (1990). Carboniferous strata of the Western Canada Sedimentary Basin. *Bulletin of Canadian Petroleum Geology*, 38(1), 178-178.
- Salvage, R.O. and Eaton, D.W., 2021. Unprecedented quiescence in resource development area allows detection of long-lived latent seismicity. *Solid Earth*, 12(3), 765-783.
- Salvage, R. O., Dettmer, J., Swinscoe, T. H. A., MacDougall, K., Eaton, D. W., Stacey, M., ... & Rhie, J. (2020a). Real-Time Monitoring of Seismic Activity in the Kiskatinaw Area, Northeastern British Columbia (NTS 093P, 094A). Tech. rep., Geoscience BC Summary of Activities 2020: Energy and Water, Geoscience BC, Report 2021-2.

- Salvage, R. O., Jia, S. Q., and Eaton, D. W. (2020). The influence of competing regional stress regimes on the generation of hydraulic fracturing-induced microseismicity. *SEG Technical Program Expanded Abstracts 2020*, Society of Exploration Geophysicists, 1294-1298.
- Schorlemmer, D., Wiemer, S., & Wyss, M. (2005). Variations in earthquake-size distribution across different stress regimes. *Nature*, 437(7058), 539-542.
- Skoumal, R. J., Ole Kaven, Jacob I. Walter (2019). Characterizing Seismogenic Fault Structures in Oklahoma Using a Relocated Template-Matched Catalog. *Seismological Research Letters*; 90 (4): 1535–1543.
- Steffen, R., Wu, P., Steffen, H., & Eaton, D. W. (2014). The effect of earth rheology and ice-sheet size on fault slip and magnitude of postglacial earthquakes. *Earth and Planetary Science Letters*, 388, 71-80.
- U.S. Geological Survey (2014): Shuttle Radar Topography Mission, digital topographic data; U.S. Geological Survey, 30 m cell, zipped hgt format, URL <<http://dds.cr.usgs.gov/srtm/>>
- Vantassel, J. P. (2020). *jpvantassel/hvsrpy: latest (Concept)*. Zenodo.
- Vasyura-Bathke, H., Dettmer, J., Steinberg, A., Heimann, S., Isken, M. P., Zielke, O., Mai, P., Sudhaus, H. and Jónsson, S. (2020). The Bayesian earthquake analysis tool. *Seismological Research Letters*, 91(2A), 1003-1018.
- Wald, D. J., Quitoriano, V., Heaton, T. H., Kanamori, H., Scrivner, C. W., & Worden, C. B. (1999). TriNet “ShakeMaps”: Rapid generation of peak ground motion and intensity maps for earthquakes in southern California. *Earthquake Spectra*, 15(3), 537-555.
- Waldhauser, F. and Ellsworth, W.L., 2000. A double-difference earthquake location algorithm: Method and application to the northern Hayward fault, California. *Bulletin of the Seismological Society of America*, 90(6), 1353-1368.
- Wiemer, S. and Wyss, M., 2000. Minimum magnitude of completeness in earthquake catalogs: Examples from Alaska, the western United States, and Japan. *Bulletin of the Seismological Society of America*, 90(4), 859-869.
- Zoback, M.D., Kohli, A., Das, I. and McClure, M.W., 2012, January. The importance of slow slip on faults during hydraulic fracturing stimulation of shale gas reservoirs. In *SPE Americas Unconventional Resources Conference*. Society of Petroleum Engineers.
- Zonneveld, J. P., & Moslow, T. F. (2018). Palaeogeographic setting, lithostratigraphy, and sedimentary framework of the Lower Triassic Montney Formation of western Alberta and northeastern British Columbia. *Bulletin of Canadian Petroleum Geology*, 66(1), 93-127.

# Appendix 1: Project Personnel

## Faculty

**Prof. David Eaton** is the former NSERC/Chevron Industrial Research Chair in Microseismic System Dynamics in the Department of Geoscience at the University of Calgary. Together with graduate students and postdoctoral fellows, his work focuses primarily on advancement of research, education and technological innovations in microseismic methods and their practical applications for resource development, with a secondary focus on the deep lithospheric structure of continents. In 2007, he rejoined the University of Calgary as Head of the Department of Geoscience, after an 11-year academic career at the University of Western Ontario. His postdoctoral research experience included work at Arco's Research and Technical Services (Plano, Texas) and the Geological Survey of Canada (Ottawa). He has over 170 publications in peer-reviewed journals and books, including articles in *Nature* and *Science*, as well as a textbook on *Passive Seismic Monitoring of Induced Seismicity*. In 2020 he was awarded the J. Tuzo Wilson medal by the Canadian Geophysical Union, which recognizes a scientist who has made outstanding contributions to the advancement of geophysical knowledge based on excellence in scientific or technical research, instrument development, industrial applications, and teaching.

**Dr. Jan Dettmer** (Diplom Geophysiker University of Hamburg 2002, PhD Earth and Ocean Science University of Victoria 2007) is an Assistant Professor in the Department of Geoscience at the University of Calgary. He was an Office of Naval Research postdoctoral fellow in 2007 and 2008, a Research Scientist at the University of Victoria from 2009 to 2013, and research fellow at the Australian National University from 2013 to 2016. Jan's research interests include seismology and acoustics. Particular areas of interest are on earthquake sources studies, underwater acoustics and sonar, seismic ambient noise studies, high performance computing on massively parallel systems, Bayesian uncertainty quantification in geophysical inverse problems, probabilistic machine learning, and parallel algorithms. Jan's research is highly multidisciplinary and includes elements of geophysics, physics, computer science, and applied mathematics. He received the 2017 A. B. Wood Medal jointly from the Institute of Acoustics (UK) and the Acoustical Society of America "For development of inverse theory and its applications to understanding seabed and ocean structures". Dr. Dettmer is a

Fellow of the Acoustical Society of America. His research led to over 50 peer-reviewed journal articles, including 19 with students as first author.

## **Staff**

**Kelly MacDougall** received her BSc in Applied Geosciences from the University of Western Ontario. She is a professional geologist with APEGA and has worked in the oil and gas industry for over 15 years. Her roles have included exploration in the WCSB, operations in the Algerian Berkine Basin, and project management of large-scale oil sand and potash exploration programs in Alberta and Saskatchewan. She currently is the Project Manager of the Microseismic Industry Consortium under the supervision of Prof. Eaton.

**Dr. Thomas H. A. Swinscoe** joined the University of Calgary in April 2020 as a GIS Specialist to provide technical support for the Microseismic Industry Consortium. He has seven years of research and three years of consulting experience working on a wide range of hydrological and geophysical projects for the private, public and voluntary sectors in Canada, Costa Rica and the UK. He obtained his PhD in Water Resource Management from the University of Leeds, UK in September 2017, his MSc in Catchment Dynamics and Management from the University of Leeds, UK in November 2011, and his BSc in Marine and Coastal Resource Management from the University of Aberdeen, UK in July 2010.

## **Postdoctoral fellows**

**Dr. Carolyn Furlong** is a postdoctoral fellow at the University of Calgary. Her research focuses on understanding the interconnection between sedimentology and stratigraphy, and how it relates to depositional processes, reservoir distribution, heterogeneities in rock fabric, and the distribution faults and fractures within the Montney Formation. She is also interested in understanding how geological characteristics enhance or hinder the occurrence of induced seismic events. She obtained her PhD in Geology from the University of Alberta in 2019. She holds a MSc in Geology from the University of Alberta and a BSc in Earth Science Education from the State University of New York College at Cortland.

**Dr. Rebecca O. Salvage** is a postdoctoral fellow at the University of Calgary. Her research focuses on the detection and analysis of seismicity identified from resource development projects and wastewater disposal, and its relationship to fault and fracture activation. She is also interested in understanding the detailed source characteristics of events and ambient seismic noise to better constrain and differentiate seismicity within seismically noisy environments. She obtained her PhD in Geophysics from the University of Leeds, UK in December 2015. She also holds a Masters degree in Geology from the University of Bristol, UK. From 2016-2018 she was a Profesor Visitante at the Observatorio Vulcanológico y Sismológico de Costa Rica, undertaking realtime monitoring, processing and analysis of tectonic and volcano seismicity in Costa Rica and Central America.

## **Graduate students**

**Zahra Esmailzadeh** is working on her PhD in Geophysics/Seismicity with Prof. Eaton at the University of Calgary. She received an MSc in Reservoir Engineering in Iran. Before returning to academia, Zahra worked several years for the National Iranian Oil Company, studying large oil and gas reservoirs. Her current research focuses on reservoir modeling, geomechanical analysis, injection-induced seismicity, and hydraulic fracturing simulation.

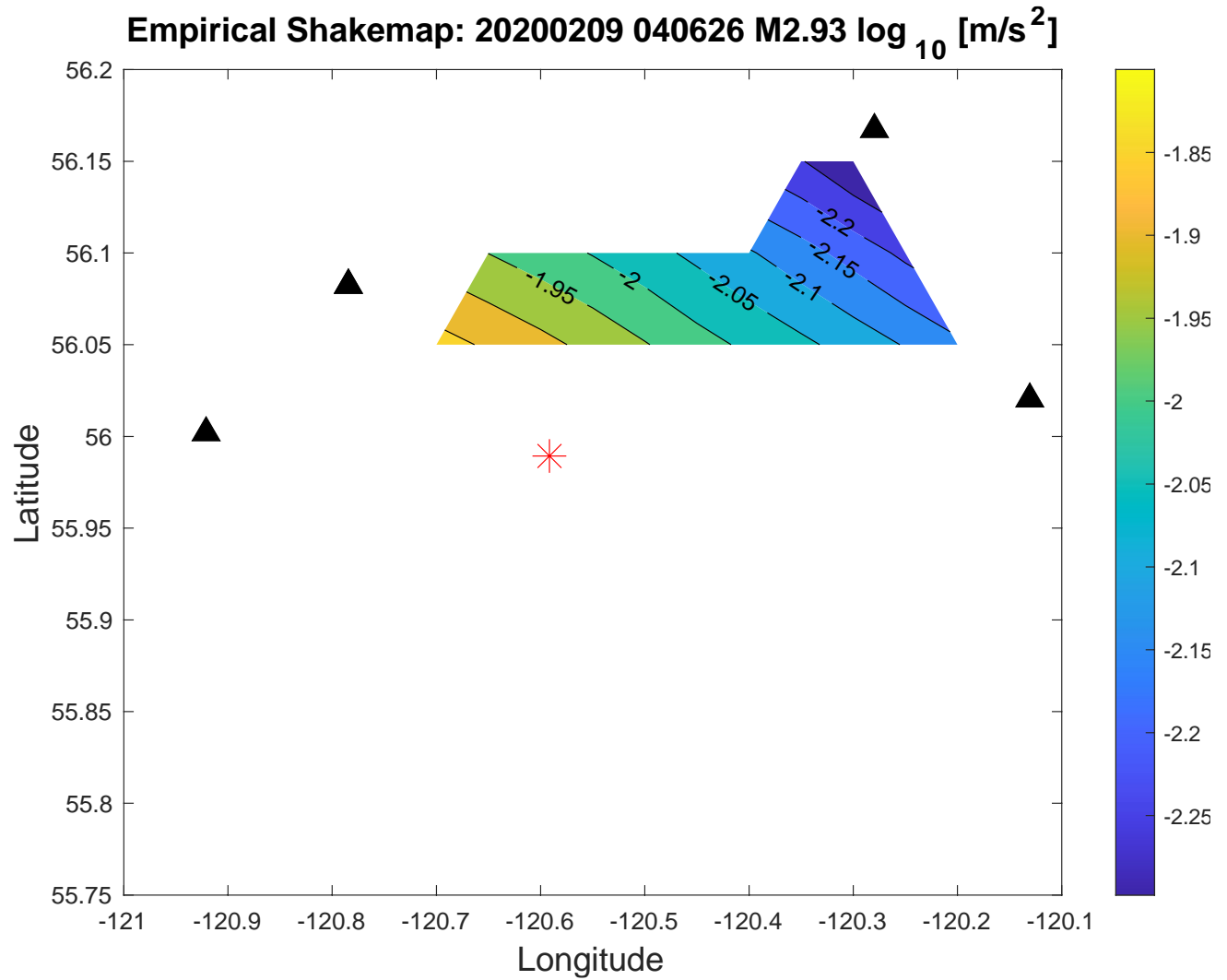
**Mahdi Hamidbeygi** is working on his MSc thesis in Geophysics/seismology with Dr. Dettmer at the University of Calgary. His research focuses on better understanding induced seismicity of KSMMA, including determining seismic source characteristics, investigating complex tectonics, and how hydraulic fracturing can affect tectonic structures. He holds a Masters's degree in seismology from the Institute of Geophysics, and a bachelor's degree in Mining Engineering from the University of Tehran in Iran.

**Prince Igweze** is a course-based MSc student in Geophysics at the University of Calgary with Dr. Eaton. He received his BSc in Physics with a major in Geophysics at Covenant University, Nigeria, and a Post Graduate Diploma in Petroleum Geoscience at Laser Geoscience School, Nigeria. Prince's current research project focuses on developing machine learning tools and applying robust quantitative

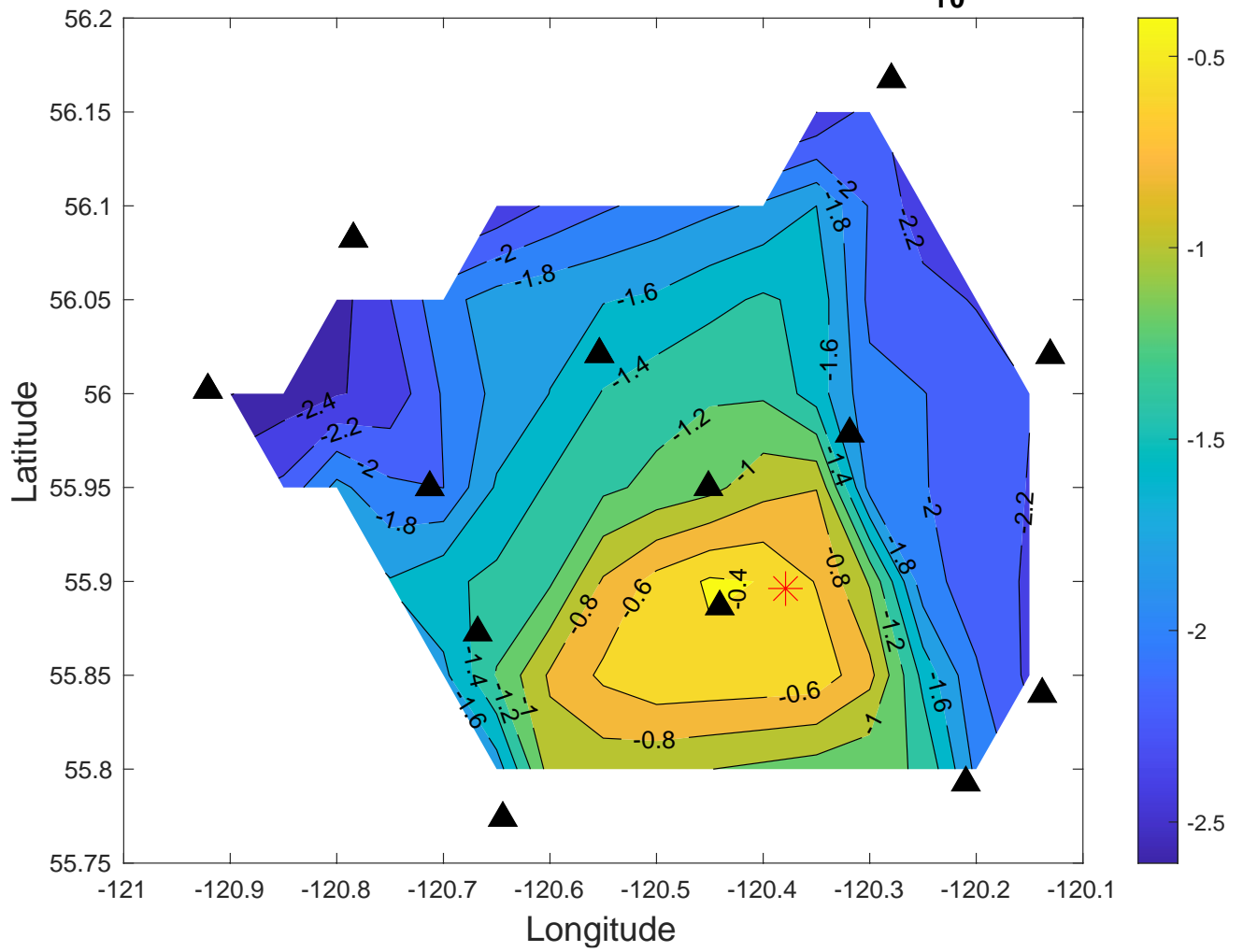
methods to study the seasonal variations in site response in the Kiskatinaw Seismic Monitoring and Mitigation Area (KSMMA). His industry experience spans involvement in oil field development projects as a Geophysicist. He is an active member of the CSEG.

**Paulina Wozniakowska** is working on her PhD in Geophysics with Dr. David Eaton at the University of Calgary. She received her MSc (2016) and BSc (2015) in Applied Geophysics at the AGH University of Science and Technology in Krakow, Poland. Paulina's current research focuses on geospatial analysis of induced seismicity. Before returning to academia, she worked in Czech Republic as a microseismic data analyst. She is a Vice President of CSEG UofC Student Chapter and 2019 and 2020 Geoscience BC Scholarship Recipient.

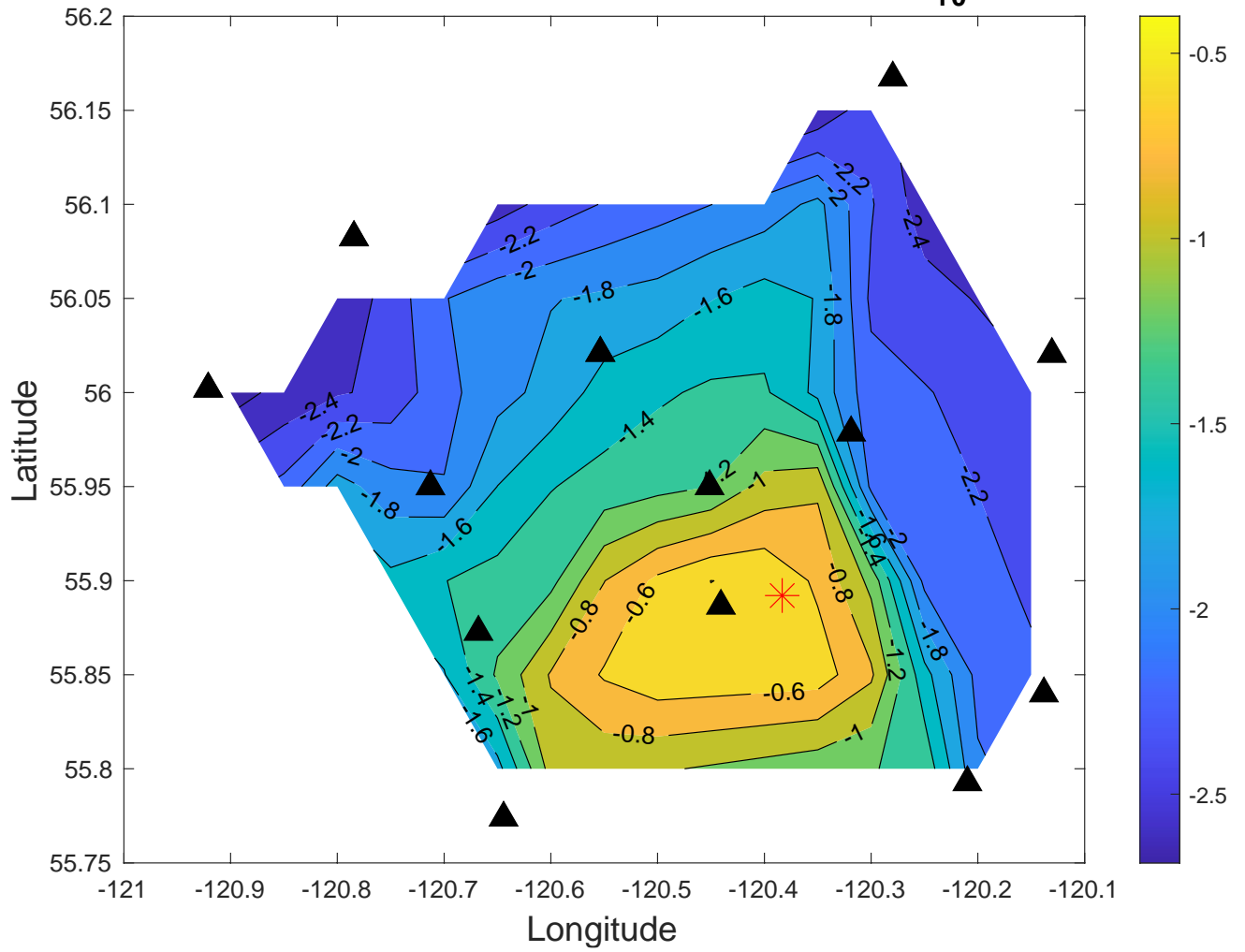
## Appendix 2: Empirical Shakemaps for the 10 largest events



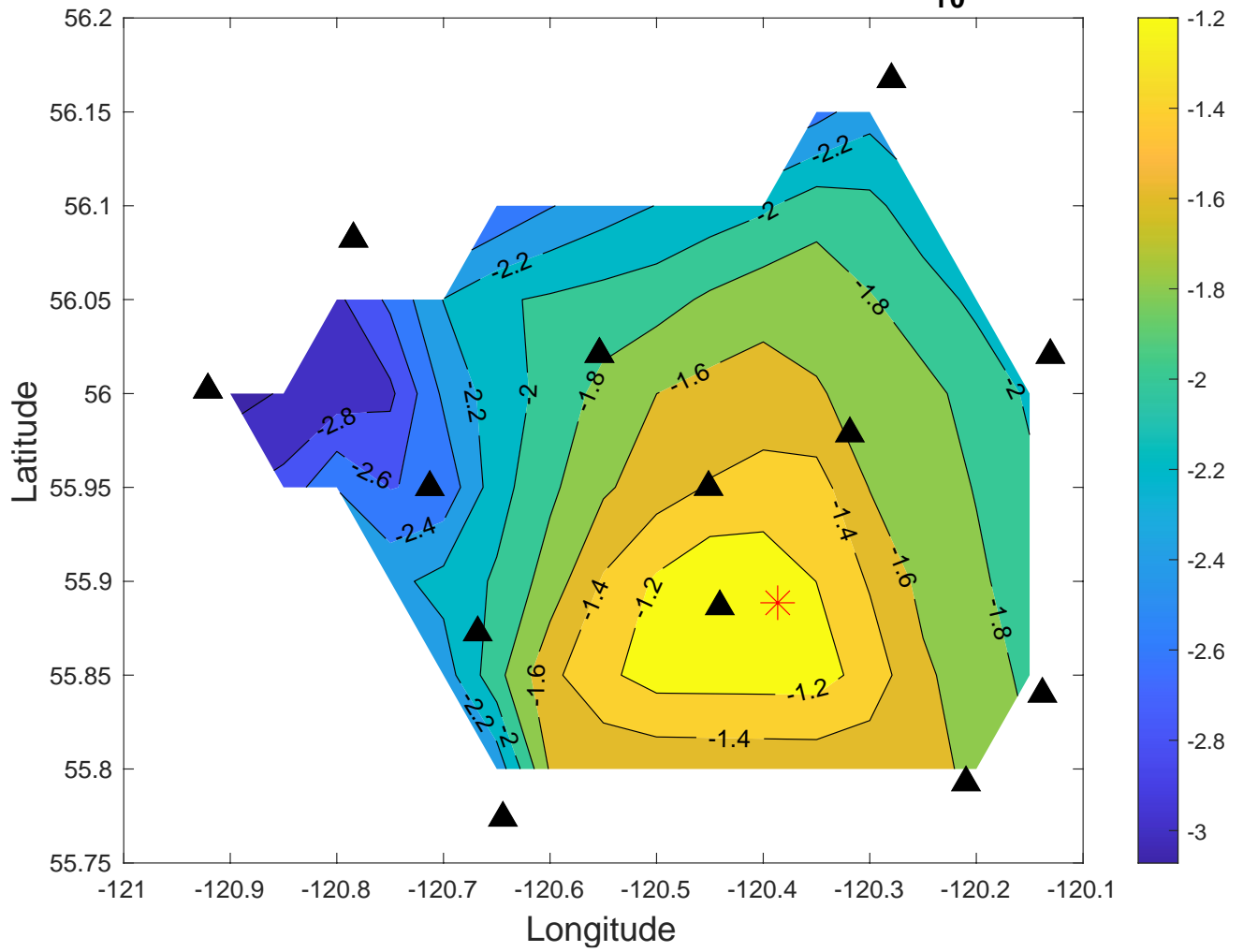
### Empirical Shakemap: 20200909 220827 M2.95 $\log_{10}$ [m/s<sup>2</sup>]



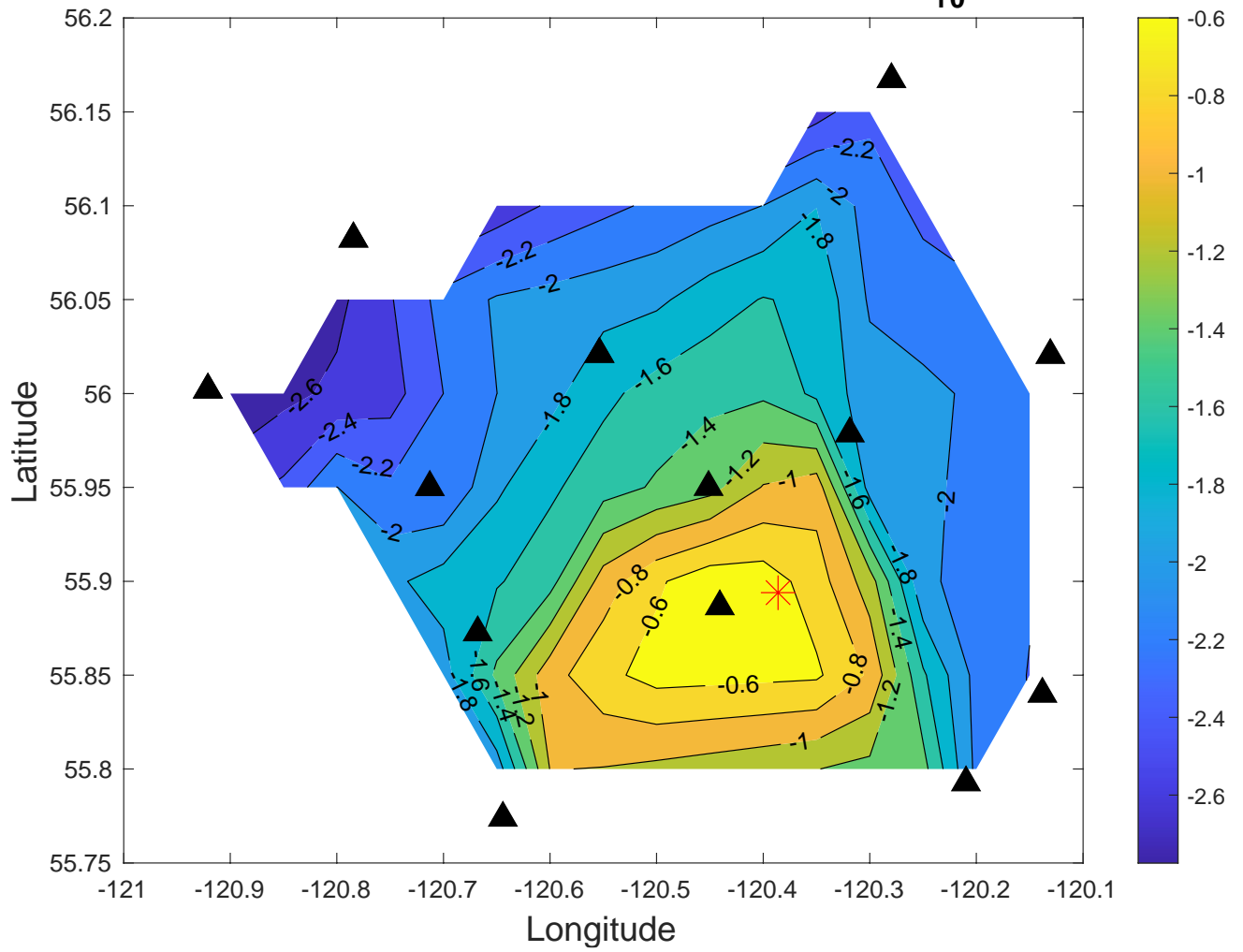
Empirical Shakemap: 20200910 002022 M2.88  $\log_{10}$  [ $\text{m/s}^2$ ]



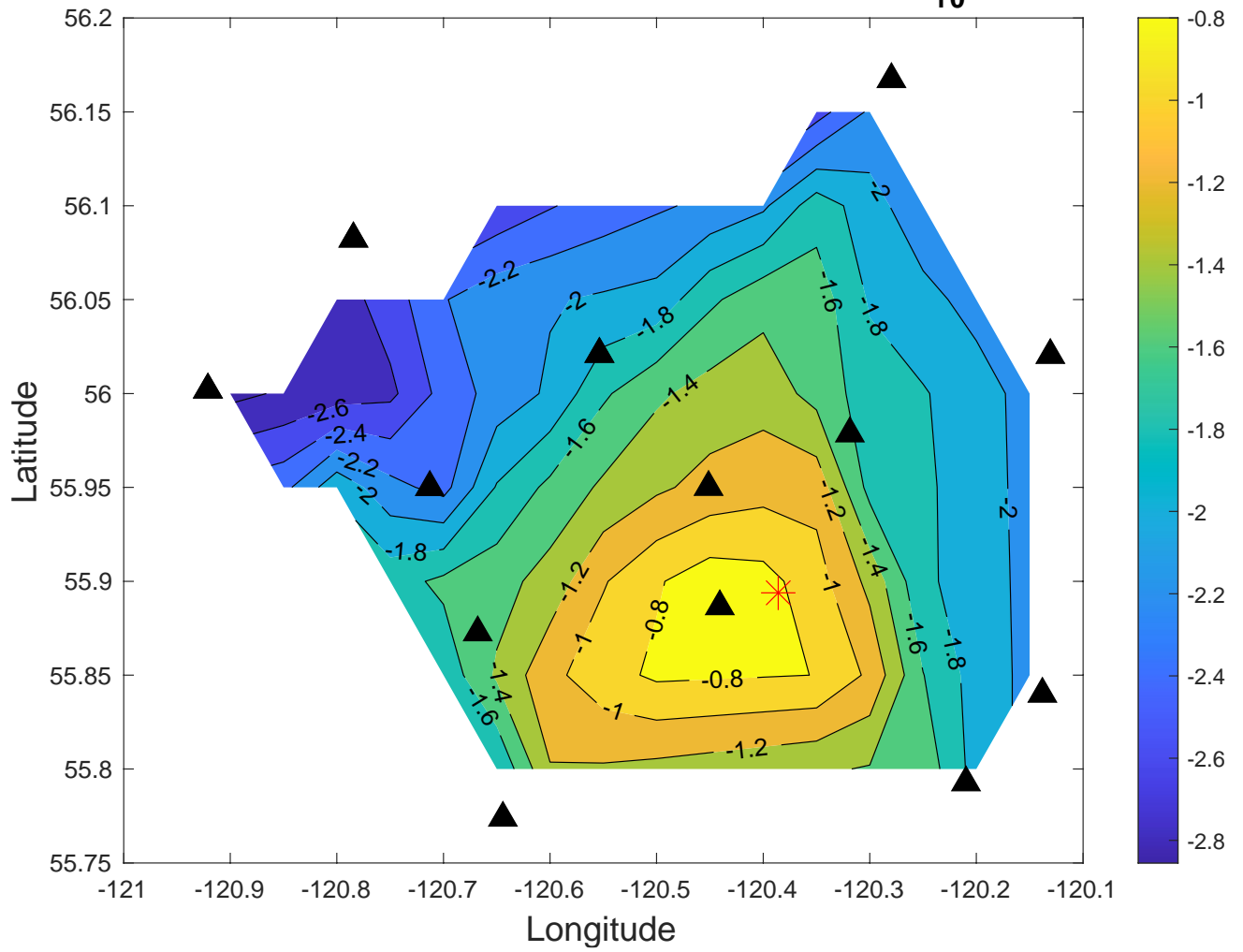
### Empirical Shakemap: 20200910 101858 M2.77 $\log_{10}$ [m/s<sup>2</sup>]



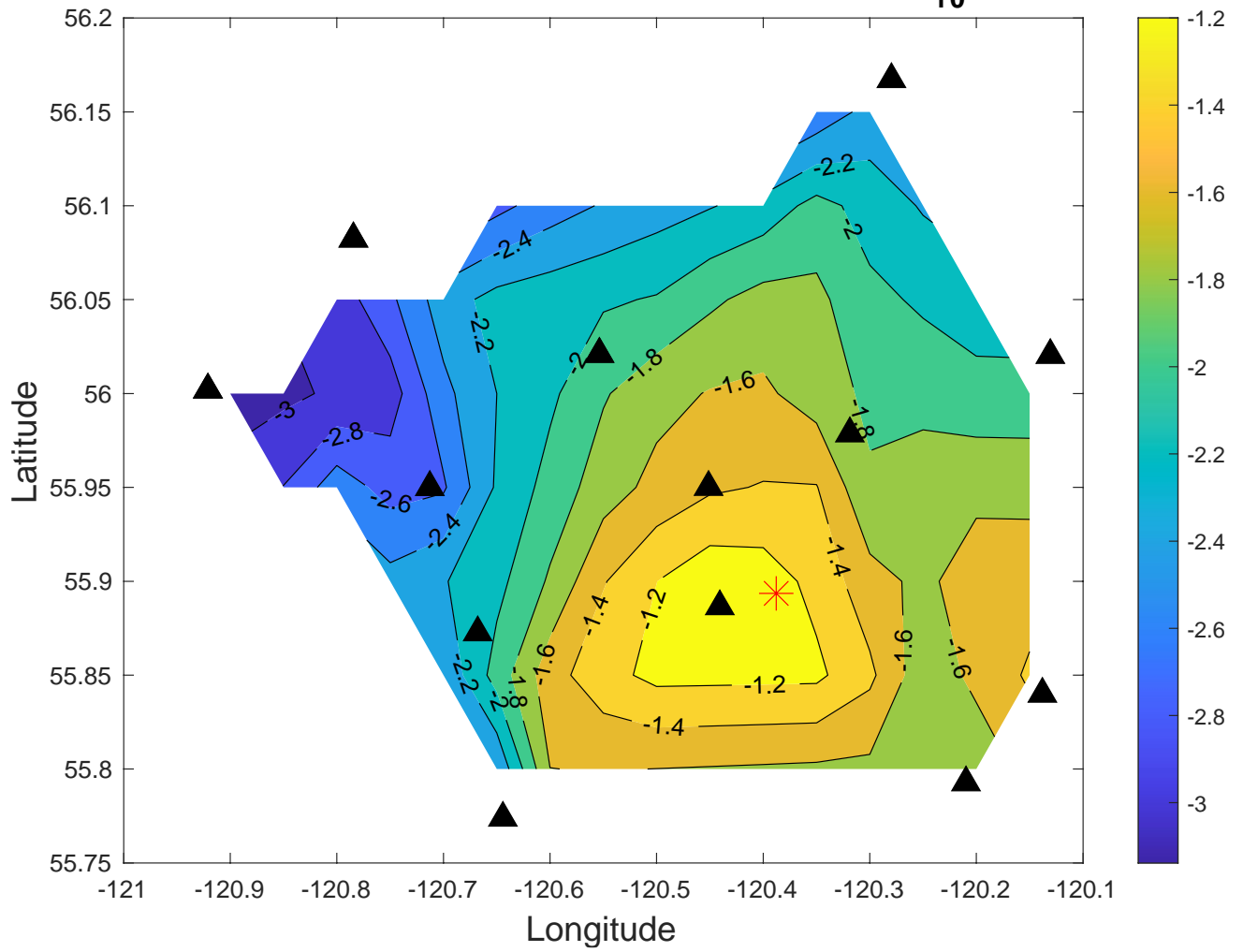
Empirical Shakemap: 20200911 002200 M2.89  $\log_{10}$  [m/s<sup>2</sup>]



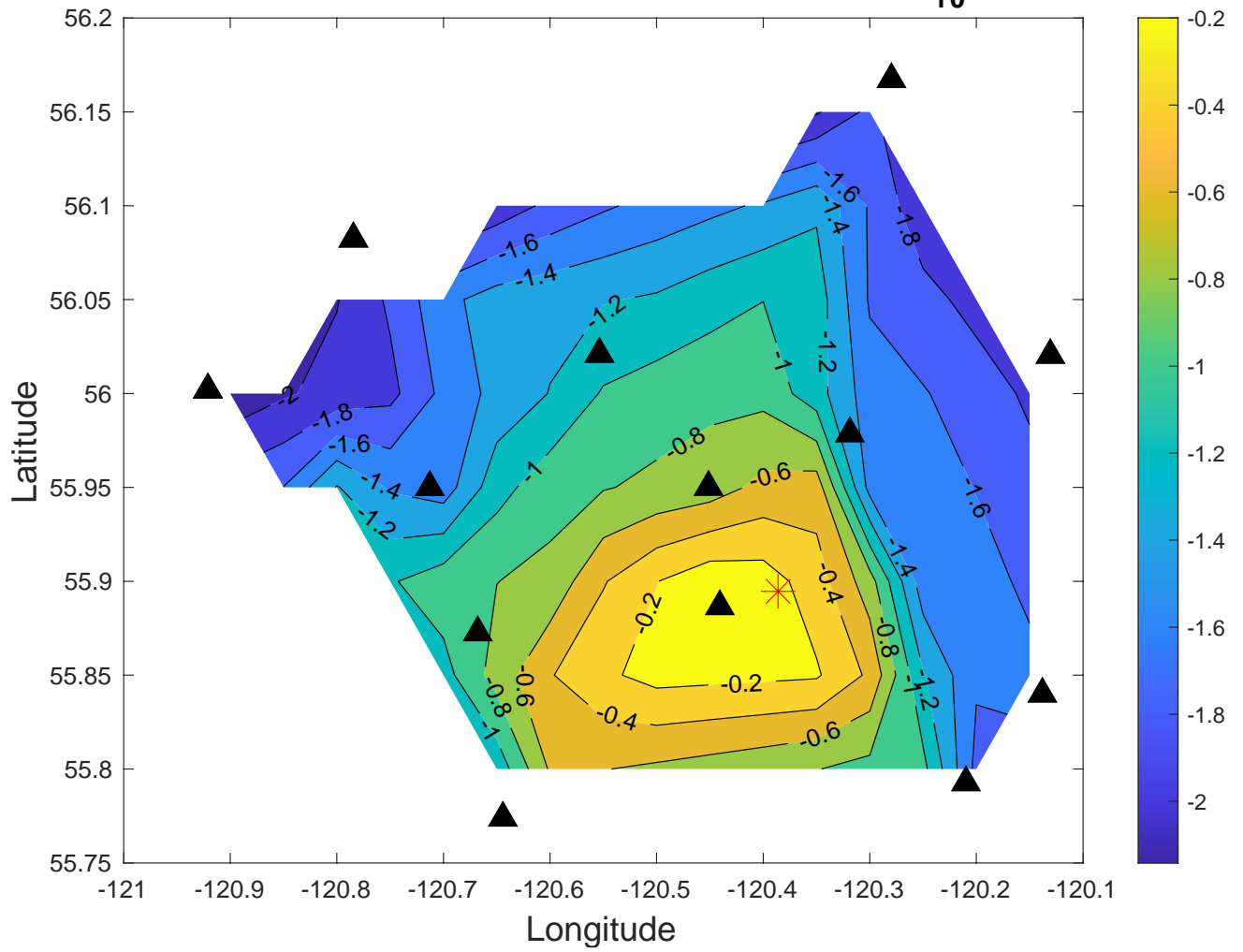
Empirical Shakemap: 20200911 003916 M2.86  $\log_{10}$  [m/s<sup>2</sup>]



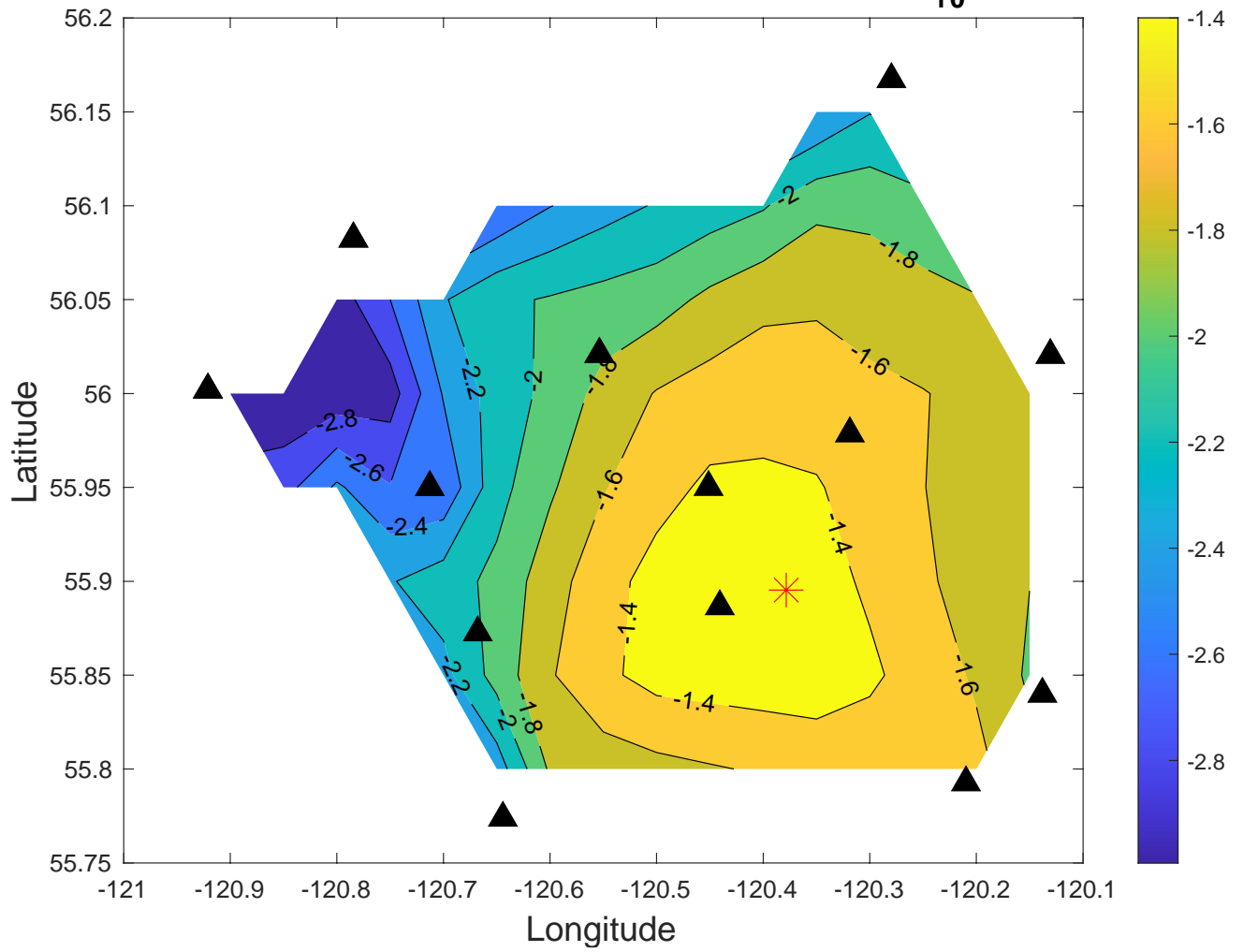
### Empirical Shakemap: 20200911 013033 M2.76 $\log_{10}$ [m/s<sup>2</sup>]



### Empirical Shakemap: 20200911 223726 M3.41 $\log_{10}$ [m/s<sup>2</sup>]



### Empirical Shakemap: 20200916 155921 M3.07 $\log_{10}$ [m/s<sup>2</sup>]



### Empirical Shakemap: 20200923 211843 M2.86 $\log_{10}$ [m/s<sup>2</sup>]

